

## RESEARCH ARTICLE

# Topological analyses of functional connectomics: A crucial role of global signal removal, brain parcellation, and null models

Xiaodan Chen<sup>1,2,3</sup> | Xuhong Liao<sup>1,2,3</sup>  | Zhengjia Dai<sup>1,2,3</sup> | Qixiang Lin<sup>1,2,3</sup> | Zhiqun Wang<sup>4</sup> | Kuncheng Li<sup>4</sup> | Yong He<sup>1,2,3</sup>

<sup>1</sup>State Key Laboratory of Cognitive Neuroscience and Learning, Beijing Normal University, Beijing, China

<sup>2</sup>Beijing Key Laboratory of Brain Imaging and Connectomics, Beijing Normal University, Beijing, China

<sup>3</sup>IDG/McGovern Institute for Brain Research, Beijing Normal University, Beijing, China

<sup>4</sup>Department of Radiology, Xuanwu Hospital of Capital Medical University, Beijing, China

## Correspondence

Xuhong Liao, State Key Laboratory of Cognitive Neuroscience and Learning, Beijing Key Laboratory of Brain Imaging and Connectomics, IDG/McGovern Institute for Brain Research, Beijing Normal University, Beijing 100875, China.

Email: liaoxuhong@bnu.edu.cn and Yong He, State Key Laboratory of Cognitive Neuroscience and Learning, Beijing Key Laboratory of Brain Imaging and Connectomics, IDG/McGovern Institute for Brain Research, Beijing Normal University, Beijing 100875, China.  
Email: yong.he@bnu.edu.cn

## Funding information

Natural Science Foundation of China, Grant/Award Numbers: 91432115, 81620108016, 81571648; Changjiang Scholar Professorship Award, Grant/Award Number: T2015027; Beijing Municipal Science & Technology Commission, Grant/Award Numbers: Z161100004916027, Z151100003915082, Z161100000216152; Fundamental Research Funds for the Central Universities, Grant/Award Numbers: 2015KJCA13, 2017XTCX04

## Abstract

Recently, functional connectome studies based on resting-state functional magnetic resonance imaging (R-fMRI) and graph theory have greatly advanced our understanding of the topological principles of healthy and diseased brains. However, how different strategies for R-fMRI data preprocessing and for connectome analyses jointly affect topological characterization and contrastive research of brain networks remains to be elucidated. Here, we used two R-fMRI data sets, a healthy young adult data set and an Alzheimer's disease (AD) patient data set, and up to 42 analysis strategies to comprehensively investigate the joint influence of three key factors (global signal regression, regional parcellation schemes, and null network models) on the topological analysis and contrastive research of whole-brain functional networks. At the global level, we first found that these three factors affected not only the quantitative values but also the individual variability profile in small-world related metrics and modularity, wherein global signal regression exhibited the predominant influence. Moreover, strategies without global signal regression and with topological randomization null model enhanced the sensitivity of the detection of differences between AD and control groups in small-worldness and modularity. At the nodal level, strategies of global signal regression dominantly influenced the spatial distribution of both hubs and between-group differences in terms of nodal degree centrality. Together, we highlight the remarkable joint influence of global signal regression, regional parcellation schemes and null network models on functional connectome analyses in both health and diseases, which may provide guidance for the choice of analysis strategies in future functional network studies.

## KEYWORDS

connectomics, graph theory, hub, modularity, small-worldness

## 1 | INTRODUCTION

Resting-state functional magnetic resonance imaging (R-fMRI) is a promising and powerful neuroimaging technique that can noninvasively measure intrinsic or spontaneous activity in the human brain (Biswal, Zerrin Yetkin, Haughton, & Hyde, 1995; Fox & Raichle, 2007). In the past 20 years, R-fMRI has been widely used to study inter-

regional functional connectivity patterns, that is, the functional connectome in healthy and diseased populations (Biswal et al., 2010; Kelly, Biswal, Craddock, Castellanos, & Milham, 2012). Specifically, with the aid of graph theory approaches, recent R-fMRI studies have demonstrated that human brain functional networks exhibit many important topological properties, such as efficient small-world properties for balanced functional segregation and integration, significant

modular structure, and densely connected hubs (Bullmore & Sporns, 2009; He & Evans, 2010; Liao, Vasilakos, & He, 2017; van den Heuvel & Sporns, 2013). Moreover, these brain network properties exhibit important correlations with physiological signatures (e.g., cerebral glucose and blood flow consumption) (Liang, Zou, He, & Yang, 2013; Tomasi, Wang, & Volkow, 2013) and individual differences in cognitive behaviors (Alavash, Doebler, Holling, Thiel, & Giessing, 2015; Cohen & D'Esposito, 2016; Liu et al., 2017), and these properties change with development, aging, and diseases (for reviews, see Cao, Huang, & He, 2017; Filippi et al., 2013; Fornito & Bullmore, 2015; Zhao, Xu, & He, 2018). Thus, the investigation of R-fMRI functional networks based on graph theory has important implications for understanding the topological mechanisms of large-scale brain networks in both healthy and diseased conditions.

It is worth noting that growing evidence from functional network studies suggests that the topological properties of R-fMRI brain networks can be influenced by different factors including specific image preprocessing (e.g., regression of the global signal), network construction (e.g., node definitions), and analysis approaches (e.g., null models for small-worldness estimation). Regarding this topic, first, several R-fMRI studies have suggested that global signal regression (GSR) can partially reduce the influence of nonneuronal signals, such as those from respiration and head motion (Birn, Diamond, Smith, & Bandettini, 2006; Power et al., 2013; Power, Plitt, Laumann, & Martin, 2016; Satterthwaite et al., 2013; Yan et al., 2013) but can simultaneously alter the correlation structure of brain networks (Murphy, Birn, Handwerker, Jones, & Bandettini, 2009). Moreover, Scholvinck, Maier, Ye, Duyn, and Leopold (2010) demonstrated that the global R-fMRI signal in monkeys is directly linked to spontaneous fluctuations in the local field potential, which suggests the underlying neural basis of global R-fMRI fluctuations. To date, controversy persists regarding whether the global R-fMRI signal should be removed during functional network studies (Murphy & Fox, 2016). Second, in current functional brain network analyses, there is no gold standard for the definition of brain nodes (Bullmore & Bassett, 2011; Wig, Schlaggar, & Petersen, 2011). Network nodes are usually defined as regions of interest (ROIs) using various parcellation approaches, including structurally constrained atlases (e.g., automated anatomical labeling [AAL]) (Tzourio-Mazoyer et al., 2002), functionally activated or parcellated regions (Craddock, James, Holtzheimer 3rd, Hu, & Mayberg, 2012; Dosenbach et al., 2010; Power et al., 2011) and randomly parcellated regions (Zalesky et al., 2010). Several studies, including ours, have demonstrated that different regional parcellations significantly affect both global and local topological parameters in brain functional networks (Fornito, Zalesky, & Bullmore, 2010; Wang et al., 2009). Third, several studies have suggested that the estimation of small-world metrics during brain network analysis depends on the choice of the null network model (e.g., topological randomization, correlation matrix randomization or time series randomization) (Hosseini & Kesler, 2013; Zalesky, Fornito, & Bullmore, 2012). Notably, specific combinations of these influencing factors have been used in topological analyses of brain networks in neuropsychiatric disorders, such as Alzheimer's disease (AD), schizophrenia, and depression (for reviews, see Dai & He, 2014; Fornito & Bullmore, 2015; Gong & He, 2015). However, the results have often been inconsistent across studies even for a single disorder.

For example, in AD research, increased and reduced local network clustering have been reported across different studies (Liu et al., 2012; Supekar, Menon, Rubin, Musen, & Greicius, 2008), and this discrepancy could be partially attributable to the selection of different combinations of these influencing factors (Dai & He, 2014). Thus, an important but unanswered question is how these key factors (i.e., GSR strategies, regional parcellation schemes, and null network models) *jointly affect* the topological properties of functional brain networks. Moreover, how these factors *jointly affect* contrastive research on brain network topology in neuropsychiatric diseases, such as AD, remains to be further elucidated.

To address these issues, in this study, we employed two R-fMRI data sets and graph-theory approaches to comprehensively investigate the joint influence of three key factors (GSR or not, regional parcellation schemes and null network models) on the topological analyses of whole-brain functional networks in healthy and diseased conditions. In Data set 1, we used R-fMRI data from 143 healthy young adults to evaluate the effects of up to 42 different analysis strategies of interest (involving combinations of two GSR strategies, seven parcellation schemes and three null network models) on the topological properties of whole-brain functional networks based on an individual difference analysis approach. In Data set 2, we used R-fMRI data from 32 AD patients as a representative disease model with network dysfunction (Dai & He, 2014; Delbeuck, Van der Linden, & Collette, 2003; Stam, 2014) and data from 38 healthy controls (HCs) to further ascertain the influences of these factors on the identification of between-group differences in topological properties based on a contrastive research strategy. Specifically, we primarily focused on the evaluation of the topological properties of brain networks in terms of small-world, modular, and nodal properties because these properties capture different organizational principles ranging from global to regional aspects and have been widely used to study topological mechanisms in healthy and diseased populations (for reviews, see Bullmore & Sporns, 2009; Dai & He, 2014; Fornito & Bullmore, 2015; Liao et al., 2017).

## 2 | MATERIALS AND METHODS

### 2.1 | Subjects

Two data sets were used in this study. The first data set (Data set 1) consisted of 146 healthy young adults from the Connectivity-based Brain Imaging Research Database (C-BIRD) at Beijing Normal University (Lin et al., 2015; Liu et al., 2017). All the participants were right-handed and had no history of neurological or psychiatric disorder. Written informed consent was obtained from each participant, and this study was approved by the Institutional Review Board of the State Key Laboratory of Cognitive Neuroscience and Learning at Beijing Normal University. Three subjects were excluded due to excessive head motion (see "Data preprocessing"). The data from the remaining 143 participants (age:  $22.8 \pm 2.3$  years; 74 females) were used for further analyses (Table 1).

The second data set (Data set 2) consisted of data from 75 right-handed subjects, including 34 AD patients and 41 HCs. The AD

**TABLE 1** Demographics of healthy young adults, AD patients, and healthy elderly adults

	Data set 1	Data set 2		<i>p</i>
	Healthy young adults ( <i>n</i> = 143)	AD ( <i>n</i> = 32)	HC ( <i>n</i> = 38)	
Age (years)	19–31 (22.8 ± 2.3)	52–86 (71.25 ± 8.63)	50–86 (68.39 ± 7.78)	.15 <sup>a</sup>
Gender (male/female)	69/74	14/18	13/25	.41 <sup>b</sup>
Education (years)	11–22 (16.2 ± 1.8)	5–16 (9.75 ± 3.14)	5–16 (9.95 ± 3.44)	.80 <sup>a</sup>
CDR	N/A	0.5 ( <i>n</i> = 14), 1 ( <i>n</i> = 18)	0	–
MMSE	N/A	10–25 (18.56 ± 3.99)	28–30 (28.63 ± 0.67)	<.001 <sup>a</sup>

Data are presented as the range of minimum–maximum values (mean ± SD). AD = Alzheimer's disease; HC = healthy control; CDR = Clinical Dementia Rating; MMSE = Mini-Mental State Examination.

<sup>a</sup> *p* value was obtained by a two-sample two-tailed *t* test.

<sup>b</sup> *p* value was obtained by a two-tailed Pearson chi-square test.

patients were recruited from the memory outpatient clinic at Xuanwu Hospital. The HCs were recruited from the local community through advertisement. All the subjects were assessed using the Clinical Dementia Rating (CDR) and were defined as HCs (CDR = 0) or as patients in the early stages of AD (18 patients had a CDR = 1, and 16 patients had a CDR = 0.5). The diagnosis of AD fulfilled the Diagnostic and Statistical Manual of Mental Disorders, 4th edition (DSM-IV) criteria for dementia and the National Institute of Neurological and Communicative Disorders and Stroke/Alzheimer's Disease and Related Disorders Association (NINCDS-ADRDA) criteria for possible or probable AD (McKhann et al., 1984). All the HCs had no neurological or psychiatric disorders, no cognitive complaints, and no neurological deficiencies, and they had Mini-Mental State Examination (MMSE) scores of 28 or higher. This data set has previously been used to study the seed-based functional connectivity of subregions of the medial and lateral parietal cortex (Wang, Xia et al., 2015; Xia et al., 2014) and functional hubs in AD (Dai et al., 2015). In addition, a subset of the data set (16 AD patients and 22 HCs) was used in two other studies (Dai et al., 2012; Wang et al., 2011). Notably, data from five subjects (2 AD patients with CDRs = 0.5 and 3 HCs) were excluded due to the failure of imaging normalization (see “Data preprocessing”). The clinical and demographic information of the remaining 70 subjects (i.e., 32 AD patients and 38 HCs) is provided in Table 1.

## 2.2 | Data acquisition

### 2.2.1 | Data set 1

MRI acquisition was performed using a SIEMENS Trio 3-Tesla scanner at Beijing Normal University. During the scan, foam padding and headphones were used to minimize head motion and scanner noises. The R-fMRI data were obtained using an echo-planar imaging (EPI) sequence with the following parameters: repetition time (TR)/echo time (TE) = 2,000 ms/30 ms; flip angle (FA) = 90°; field of view (FOV) = 200 × 200 mm<sup>2</sup>; matrix = 64 × 64; slice number = 33; voxel size = 3.13 × 3.13 × 3.5 mm<sup>3</sup>; gap = 0.7 mm; and 200 volumes. Prior to scanning, all the participants were instructed to keep their eyes closed, relax their mind, and not move during the scanning procedure. The T1-weighted data were acquired using sagittal three-dimensional (3D) magnetization prepared rapid gradient echo (MPRAGE) sequences with the following parameters: TR/TE = 2,530 ms/3.39 ms; FA = 7°;

FOV = 256 × 256 mm<sup>2</sup>; matrix = 256 × 256; slice number = 144; and voxel size = 1 × 1 × 1.33 mm<sup>3</sup>.

### 2.2.2 | Data set 2

MRI acquisition was performed on a SIEMENS Trio 3-Tesla scanner at Xuanwu Hospital. During the scan, foam padding and headphones were used to minimize head motion and scanner noises. The R-fMRI data were obtained using an EPI sequence with the following parameters: TR/TE = 2,000 ms/40 ms; FA = 90°; FOV = 240 × 240 mm<sup>2</sup>; matrix = 64 × 64; slice number = 28; voxel size = 3.75 × 3.75 × 4 mm<sup>3</sup>; gap = 1 mm; and 239 volumes. Prior to scanning, all the participants were instructed to keep their eyes closed, relax their mind, and not move during the scanning procedure. According to a simple questionnaire after the scan, all the subjects refrained from falling asleep during the scan. Structural images were collected using a sagittal 3D MPRAGE sequence with the following parameters: TR/TE = 1,900 ms; inversion time = 900 ms; FA = 9°; FOV = 256 × 256 mm<sup>2</sup>; matrix = 256 × 256; slice number = 176; and voxel size = 1 × 1 × 1 mm<sup>3</sup>.

## 2.3 | Data preprocessing

All R-fMRI data were preprocessed using Statistical Parametric Mapping software (SPM8, The MathWorks Inc., Natick, MA; <http://www.fil.ion.ucl.ac.uk/spm/>) and the Data Processing Assistant for Resting-State fMRI (DPARSF, Yan & Zang, 2010). Data set 1 and Data set 2 were separately preprocessed using similar procedures as follows.

### 2.3.1 | Data set 1

The first 10 volumes were discarded for scanner stabilization and to allow the subjects to adapt to the scanner. The remaining data were corrected for the acquisition time delay between slices within a volume and were then realigned to the first volume to correct for head motion. Three subjects were excluded due to excessive head motion (greater than 2 mm or 2° in any direction). Mean framewise displacement (FD, Power, Barnes, Snyder, Schlaggar, & Petersen, 2012) was estimated for each subject to characterize the transient head motion. The resulting images were further spatially normalized to the Montreal Neurological Institute (MNI) space using the parameters estimated from T1 unified segmentation (Ashburner & Friston, 2005) and were resampled into 3-mm isotropic voxels. Then, the spatially normalized images underwent linear trend removal and nuisance signal

regression, wherein 24 head motion parameters (Friston, Williams, Howard, Frackowiak, & Turner, 1996), white matter, cerebrospinal fluid, and global brain signals, were regressed out from the time course of each voxel. The residual signals were further temporally band-pass filtered (0.01–0.1 Hz) to decrease the effects of low-frequency drifts and high-frequency physiological noises.

### 2.3.2 | Data set 2

Data set 2 was preprocessed in the same manner as Data set 1 with the exceptions of the use of head motion exclusion criterion and a spatial normalization strategy that are relevant to the elderly. Using a head motion criterion of 3 mm and 3°, no subjects were excluded. This relatively loose head motion criterion was used for the AD patients and HCs because it is more difficult for the elderly to remain still than it is for healthy young adults. During spatial normalization, the realigned images were spatially normalized to a custom space that allowed the reduction of inaccuracies in the spatial normalization of the functional volumes caused by gray matter atrophy in AD subjects. Specifically, the individual T1-weighted structural images were first coregistered to the mean realigned functional images using a linear transformation and were then segmented into gray matter, white matter, and cerebrospinal fluid tissues using unified segmentation algorithms (Ashburner & Friston, 2005) with the priori SPM tissue maps as reference images. The resulting individual tissue images were nonlinearly registered into the MNI space according to the parameters estimated during the unified segmentation and were then averaged across all the subjects to generate custom gray matter, white matter, and cerebrospinal fluid templates. Then, the individual T1-weighted images were segmented again using the custom tissue templates generated above as reference images through the unified segmentation algorithms. Then, the motion-corrected functional images were normalized to the custom space by applying the transformation parameters that were estimated during the second unified segmentation and were resampled to 3-mm isotropic voxels. Notably, five subjects (2 AD patients and 3 HCs) were excluded from the subsequent

analyses due to the failure of image normalization, which may have been caused by image artifacts or severe gray matter atrophy.

Notably, during the preprocessing procedures described above, we performed GSR during the nuisance regression. To assess the influence of the global brain signal on the topological architecture of the brain functional networks, we also preprocessed both data sets without GSR during nuisance regression.

### 2.4 | Whole-brain network construction

Before the whole-brain network construction, a custom gray matter mask with a gray matter probability above 0.2 was first generated separately for each data set. This mask consisted of cortical and subcortical regions that were fully covered during the R-fMRI scanning for all the subjects. The cerebellum was not considered here because it was not fully covered during the R-fMRI scanning. Within this gray matter mask, functional brain networks were constructed at a macroscopic scale for each subject with nodes denoting the ROIs obtained from the following parcellation schemes.

Here, we used seven different regional parcellation schemes to define brain network nodes: three structurally constrained schemes, which included the Brodmann atlas with 82 ROIs (Brodmann-82) (Brodmann, 1909), the automated anatomical labeling atlas with 90 ROIs (AAL-90) (Tzourio-Mazoyer et al., 2002) and the Harvard and Oxford atlas with 112 ROIs (HOA-112) (Kennedy et al., 1998; Makris et al., 1999); three functionally defined schemes, which included the Dosenbach template of 160 ROIs (Dosenbach-160) (Dosenbach et al., 2010), the Craddock template of 200 ROIs (Craddock-200) (Craddock et al., 2012), and the Power template of 264 ROIs (Power-264) (Power et al., 2011); and one randomly defined scheme, which included 1,024 ROIs of uniform size (Random-1024) that were obtained through a random parcellation algorithm (Zalesky et al., 2010; Figure 1). For Data set 2, all the regional parcellation images in the MNI space were transformed to the custom space using the transformation parameters estimated for the spatial normalization of the priori SPM gray matter tissue map to the custom space. This

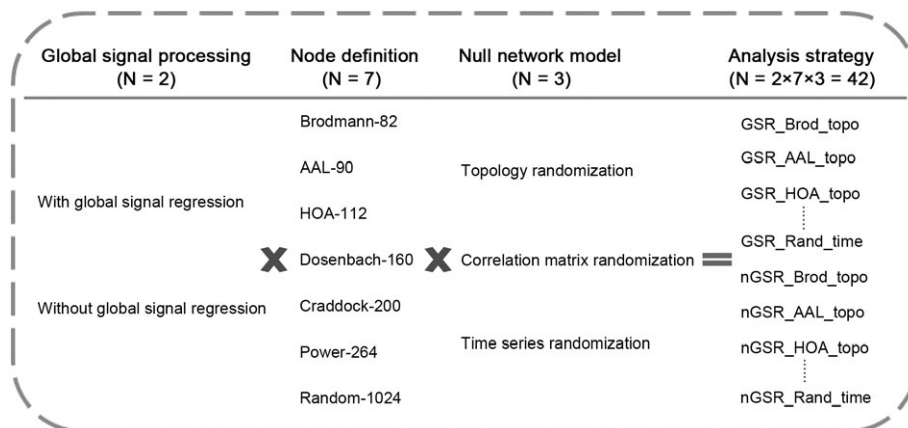


**FIGURE 1** Schematic diagram of 42 analysis strategies used in this study. These analysis strategies were generated by combining three factors for data preprocessing, network construction, and network analysis, including two global signal regression strategies, seven regional parcellation schemes, and three null network models. In the naming scheme of the analysis strategies, “Brod,” “AAL,” “HOA,” and “Rand” represent the Brodmann-82, AAL-90, HOA-112, and Random-1024 parcellation schemes, respectively; “topo” and “time” indicate topological randomization and time series randomization, respectively; and “GSR” and “nGSR” indicate with and without global signal regression, respectively

procedure allowed the precise localization of the ROI positions in the custom space and reduced the inaccuracy of the subsequent network analysis caused by gray matter atrophy in the elderly population. During the construction of the brain networks, for each parcellation, we excluded ROIs that located outside the cerebrum (Supporting Information Table S1).

Given a parcellation scheme with  $N$  nodes, we constructed individual functional brain networks for each subject. Briefly, we generated the time course of each ROI by averaging the preprocessed time courses of all voxels within the ROI. Then, we generated a symmetric  $N \times N$  correlation matrix by calculating the Pearson's correlation coefficients between the time courses of each pair of ROIs. Consequently, for each subject, we obtained 14 node-by-node correlation matrices based on the seven parcellation schemes (i.e., 7 with GSR and 7 without GSR). Because the physiological interpretation of negative correlations is ambiguous (Murphy & Fox, 2016), functional connections with negative correlation values were not considered here. This approach is widely used in current functional brain network studies of healthy and diseased populations (Bassett, Meyer-Lindenberg, Achard, Duke, & Bullmore, 2006; Buckner et al., 2009; Doucet, Bassett, Yao, Glahn, & Frangou, 2017; Liang et al., 2013; Power, Schlaggar, Lesov-Schlaggar, & Petersen, 2013; van den Heuvel et al., 2017). Then, we generated binary functional brain networks by thresholding these correlation matrices with two commonly used thresholding approaches, including a fixed-density thresholding and a fixed-correlation thresholding. These two approaches characterize the topological organization of functional networks from different perspectives (Bullmore & Bassett, 2011; He et al., 2009; van den Heuvel et al., 2017). The former generated individual functional networks with the same number of edges and allowed an examination of the relative network topology of each subject. The latter constructed individual functional networks with edges exceeding a given correlation threshold and allowed an examination of the absolute network topology. In the main results, we first analyzed both the global and local topological organizations of the functional brain networks with a density of 15% to ensure the high connectedness of the brain networks and exclude spurious correlations where possible. Then we replicated the main analysis by generating functional networks with a fixed-correlation threshold of  $r = .2$ . To explore the potential influence of thresholding strategies, we verified our results in functional networks that were constructed at other density levels (i.e., 10, 20, and 30%) (see "Validation analysis").

## 2.5 | Network topology analysis

For each subject, we calculated the topological properties of the whole-brain functional networks using a graph theoretical network analysis toolbox (GRETNA) developed by our research group (<http://www.nitrc.org/projects/gretna>; Wang, Wang et al., 2015). We computed five small-world related metrics (i.e., clustering coefficient [ $C_p$ ], characteristic path length [ $L_p$ ], normalized clustering coefficient [ $\gamma$ ], normalized path length [ $\lambda$ ], and small-worldness [ $\sigma$ ]) and the modularity  $Q$  for the individual functional networks (Bullmore & Sporns, 2009; He & Evans, 2010; Liao et al., 2017). The clustering coefficient ( $C_p$ ) of a network equals the average of the clustering coefficients of all nodes in the network, where the nodal clustering coefficient measures

the ratio of existing connections among neighbors of a node to the maximum number of possible connections. The characteristic path length ( $L_p$ ) of the network equals the average minimum number of connections needed to link any two nodes in the network. The normalized clustering coefficient ( $\gamma$ ) and normalized path length ( $\lambda$ ) are generated by normalizing the  $C_p$  and  $L_p$  values, respectively, of the observed networks to the mean value of the same metrics in 100 null networks. Small-worldness ( $\sigma$ ) is the ratio of  $\gamma$  to  $\lambda$  and quantitatively measures the extent of small-worldness of the network (Humphries, Gurney, & Prescott, 2006; Watts & Strogatz, 1998). Typically, a small-world network exhibits high local clustering ( $\gamma \gg 1$ ) and short path length ( $\lambda \sim 1$ ), which leads to a  $\sigma > 1$  (Humphries et al., 2006). Modularity ( $Q$ ) reflects the extent to which a network is organized into a modular or community structure (Newman & Girvan, 2004). Specifically, we detected modular structures for each subject using a spectral optimization algorithm (Newman, 2006; Newman & Girvan, 2004) and computed the modular index (i.e., modularity) based on the subject-specific modular structures as follows (Newman, 2004):

$$Q(p) = \sum_{s=1}^{N_c} \left[ \frac{l_s}{m} - \left( \frac{d_s}{2m} \right)^2 \right],$$

where  $N_c$  is number of modules,  $m$  denotes total number of edges in the network,  $l_s$  indicates total number of edges within module  $s$ , and  $d_s$  is total degree value of the nodes in module  $s$  (see Supporting Information Figure S1 for representative modular structures). Moreover, for each node  $i$  in a brain network, we also estimated its nodal degree centrality  $Deg(i)$  as the number of nodes that directly linked with that node.

Notably, choosing different null network models can affect the estimations of the small-world network parameters (i.e.,  $\gamma$ ,  $\lambda$ , and  $\sigma$ ). We evaluated the effects of three different null network models (i.e., topological randomization, correlation matrix randomization, and time series randomization; Zalesky et al., 2012) on the estimation of small-world metrics. Briefly, topological randomization, the most widely used strategy for generating null networks in current brain network studies, randomly rewires the connections between nodes while preserving the numbers of nodes and edges, and the nodal degree distribution of the original network (Maslov & Sneppen, 2002). During correlation matrix randomization, null correlation matrices that preserved the mean value and the standard deviation (SD) of the original correlation distribution were randomly generated using the brute-force approach (Zalesky et al., 2012). Specifically, given a parcellation of  $N$  ROIs,  $N$  independent random vectors ( $X_i$ ,  $i = 1, 2, \dots, N$ ) were first generated, each following a standard normal distribution (i.e., mean = 0 and SD = 1). To ensure the nonzero correlation between these vectors, all these vectors  $X_i$  had been added a common random vector  $Y$  via  $X_i + cY$ , wherein  $Y$  followed a standard normal distribution and  $c$  was a positive weighted coefficient. Then, a null correlation matrix was generated by calculating the correlation between all possible pairs of random vectors. By separately adjusting the coefficient  $c$  and the number of time points contained in the random vectors, we were able to make the null correlation matrix exhibit the same mean and SD as the empirical matrix. Then, we obtained the null networks by thresholding these null correlation matrices with the same approach as the original brain networks. During time series

randomization, randomized time courses were independently generated for each ROI by applying the Fourier transform to the observed regional time series, randomizing the phases and then applying the inverse Fourier transform (Theiler, Eubank, Longtin, Galdrikian, & Farmer, 1992). Then, we generated Pearson correlation matrices by computed the correlation coefficients between any pair of randomized ROI time courses. These matrices were further thresholded into null networks with the same approach as the original brain networks.

Overall, for each subject, four null network-independent metrics, that is,  $C_p$ ,  $L_p$ ,  $Q$ , and  $Deg(i)$ , were estimated under 14 analysis strategies (i.e., GSR or not  $\times$  7 parcellation schemes), whereas three null network-dependent metrics of  $\gamma$ ,  $\lambda$ , and  $\sigma$  were estimated under 42 analysis strategies (i.e., GSR or not  $\times$  7 parcellation schemes  $\times$  3 null network models). Here, for simplicity of description, "one analysis strategy" refers to one combination of these three factors. For example, the GSR-AAL-topo analysis strategy denotes the use of GSR procedure for image preprocessing, AAL-90 parcellation for network node definition and topological randomization for null network generation (Figure 1).

## 2.6 | Assessment of the influences of three key factors (Data set 1 and Data set 2)

To evaluate the effects of these three factors (GSR strategies, regional parcellation schemes, and null network models) on brain functional network analysis, we performed the following two analyses: (a) we statistically compared the quantitative values of every brain network metric among the different analysis strategies, and (b) we examined which factor exhibited the largest effect on topological analyses of brain networks by assessing the relationships among different analysis strategies using an individual difference analysis approach (see below).

### 2.6.1 | Influence of three factors on functional network metrics (Data set 1 and Data set 2)

#### Data set 1

To evaluate the influence of three factors (GSR strategy, parcellation scheme, and null network model) on brain network properties in healthy young adults, we separately performed repeated-measures analyses of variance (rmANOVA) on each network metric (i.e.,  $C_p$ ,  $L_p$ ,  $\gamma$ ,  $\lambda$ ,  $\sigma$ , and  $Q$ ). Specifically, two-way rmANOVA with the main factors of GSR and parcellation scheme was performed on  $C_p$ ,  $L_p$ , and  $Q$ , the estimations of which were independent of the choice of the null network models. Three-way rmANOVA was performed on  $\gamma$ ,  $\lambda$ , and  $\sigma$ , the estimations of which depended on all three factors mentioned above. All the statistics were Bonferroni corrected for multiple comparisons across the six global network metrics considered. Significance was set at  $p < 0.05$ . Notably, we did not quantify the influence of these three factors on nodal degree centrality because the nodes across different parcellation schemes were difficult to match due to their different spatial locations and network sizes.

#### Data set 2

Consistent with Data set 1, we separately performed the same statistical analyses for the HCs and AD patients.

### 2.6.2 | Relationships among the different analysis strategies based on individual difference analysis approaches (Data set 1 and Data set 2)

#### Data set 1

To further examine the potential influences of the three factors on topological analyses of functional networks, we compared the relationships among different analysis strategies using an "individual difference analysis" approach (Zhong, He, & Gong, 2015). Briefly, for each global network metric (i.e.,  $C_p$ ,  $L_p$ ,  $\gamma$ ,  $\lambda$ ,  $\sigma$ , and  $Q$ ), we first characterized its individual differences by estimating the inter-subject variation profile under every analysis strategy. Then, we evaluated the similarities in the individual differences among the different analysis strategies by calculating the across-subject Pearson's correlation of this metric between each pair of strategies and thus generated a symmetric strategy-to-strategy similarity matrix. A high correlation value between two strategies indicated highly similar inter-subject variation profiles under these two strategies. Consequently, we obtained  $14 \times 14$  strategy-to-strategy similarity matrices (i.e., 2 GSR strategies  $\times$  7 parcellation schemes) for  $C_p$ ,  $L_p$ , and  $Q$ , and  $42 \times 42$  strategy-to-strategy similarity matrices (2 GSR strategies  $\times$  7 parcellation schemes  $\times$  3 null network models) for  $\gamma$ ,  $\lambda$ , and  $\sigma$ .

To quantify the convergence and divergence of the individual difference profiles between different analysis strategies, we further performed a hierarchical cluster analysis on the strategy-to-strategy similarity matrix. Briefly, the similarity matrix between strategies was converted into a distance matrix (i.e.,  $1 - \text{similarity matrix}$ ). Then, we applied the average linkage agglomerative algorithm (Sokal, 1958) to the distance matrix. This bottom-up agglomerative approach treated each analysis strategy as a separate cluster at the initial step and then progressively merged the pair of clusters with the minimum distance into a new cluster until only one cluster was reached. During each step, the distance between any two clusters were updated and defined as the average distance between strategies in the first cluster and strategies in the second cluster. The hierarchical clustering results were displayed in a dendrogram that showed the merging process of clusters at the iterative steps. Strategies in the same cluster were more similar in individual differences profiles than those in different clusters. This procedure allowed us to distinguish the influence of these three factors by identifying the factors that dominated the hierarchical clustering.

#### Data set 2

We performed the same individual difference analysis and hierarchical cluster analysis for the healthy elders and AD patients, separately, as described for Data set 1.

## 2.7 | Identifying between-group differences in brain network metrics under different analysis strategies (Data set 2)

Using Data set 2, we further assessed the influences of different analysis strategies on the detection of between-group differences (AD vs. HC) in topological properties of functional networks, including  $C_p$ ,  $L_p$ ,  $\gamma$ ,  $\lambda$ ,  $\sigma$ ,  $Q$ , and  $Deg(i)$ . Notably, a very recent study found that between-

group differences in the global properties of functional networks (e.g., clustering coefficient) can be biased by the differences in overall functional connectivity of the functional correlation matrices (van den Heuvel et al., 2017). To address this issue, we calculated the overall functional connectivity for each subject as the mean value of all the positive correlations in the functional correlation matrix under each of the 14 analysis strategies (i.e., 2 GSR strategies  $\times$  7 parcellation schemes) and then tested their differences between two groups with age, gender, and mean FD included as covariates.

### 2.7.1 | Global topology

For each analysis strategy, we assessed the between-group difference in every global metric of interest (i.e.,  $C_p$ ,  $L_p$ ,  $\gamma$ ,  $\lambda$ ,  $\sigma$ , and  $Q$ ) using general linear regression with gender, age, and mean FD included as covariates. Because we aimed to compare the results among different strategies, the between-group differences were corrected under each analysis strategy using Bonferroni correction for six global network metrics of interest. Effect sizes of the significant differences were assessed in terms of Cohen's  $d$  value (Cohen, 1988) with the classifying criteria (Sawilowsky, 2009): 0.2–0.5 indicates small; 0.5–0.8 indicates medium; 0.8–1.2 indicates large.

### 2.7.2 | Local topology

For each analysis strategy, we identified the functional hubs for each group separately and further assessed between-group differences in regional properties using nodal degree centrality. First, for each group (i.e., AD patients and HCs), we identified the hub regions of the functional networks under each of the 14 strategies (2 GSR strategies  $\times$  7 parcellation schemes) at the group level. Briefly, a group-level degree centrality map was generated for each group by averaging individual degree centrality maps across subjects. Then, the hub regions were defined as nodes showing a relatively large degree centrality with a criterion of one  $SD$  above the mean value across the brain. Because previous studies have suggested that the global signal can remarkably affect the spatial pattern of hubs (Liao et al., 2013; Sepulcre et al., 2010), we assessed the consistency of hub distributions across different parcellation schemes under two conditions (i.e., with and without GSR) separately. Specifically, for each condition (i.e., with or without GSR), we calculated an occurrence probability map as hubs across seven parcellation schemes. The occurrence probability value of a voxel was defined as the number of parcellation schemes under which that voxel was detected as a hub divided by the total number of parcellation schemes containing this voxel. In addition, to quantify the influence of the GSR strategy, for each parcellation, we also calculated the spatial similarity of the group-level nodal degree maps between two conditions (i.e., with and without GSR) using Pearson's correlations across nodes. Second, we detected brain regions with significant between-group differences in degree values under seven parcellation strategies with GSR and without GSR separately. For each parcellation, between-group differences in nodal degree were corrected with a false-positive correction across  $N$  ROIs ( $p < 1/N$ ). This correction indicated that less than one false-positive regional result was expected per parcellation at this threshold (Lynall et al., 2010). To assess the consistency of regions with significant between-group differences across different parcellation

schemes, we obtained an occurrence probability map of significant between-group differences across seven parcellation schemes for each GSR condition (i.e., with and without GSR). The occurrence probability value of a voxel was defined as the number of parcellation schemes showing significant between-group differences at this voxel divided by the total number of parcellation schemes containing this voxel.

## 2.8 | Validation analysis

We evaluated whether the main findings were influenced by head motion or different functional network construction strategies (including varying network densities and network types). In addition, we performed a split-half analysis on Data set 1 to validate whether the significant between-group differences (AD vs. HC) in global network metrics were artifacts due to specific combinations of the three methodological factors. The relevant procedures are described as follows. (a) *Head motion*: previous studies have suggested that the influence of head motion cannot be completely removed by nuisance regression strategies (Power et al., 2012; Van Dijk, Sabuncu, & Buckner, 2012) and therefore affects the GSR and functional network topological properties (Power, Schlaggar, & Petersen, 2015; Yan, Craddock, He, & Milham, 2013). In other words, the extent of head motion may contribute to individual differences in functional network metrics. To assess the reliability of the individual difference analysis approach, in Data set 1, we re-estimated the strategy-to-strategy similarity matrices of the individual differences in the global network metrics using partial correlations controlling for the head motion parameter of mean FD. (b) *Network density*: in the main analysis, individual binary functional networks were generated using a fixed-density thresholding approach with a density of 15%. To investigate the potential effects of network density values, we validated the main results at other density levels of 10, 20, and 30%. (c) *Network type*: binary networks were used in the main analysis in which edge weights were ignored. To explore the potential influence of edge weights, we also constructed weighted networks with a fixed-density threshold (i.e., 15%) and then re-performed all the analyses. (d) *Reliability of the detection of between-group differences*: here, we compared the between-group differences (AD vs. HC, Data set 2) in six global network metrics across different analysis strategies to investigate their sensitivities in the between-group comparison. However, we are not sure whether the observed between-group differences (AD vs. HC) were reliable or artifacts introduced by the numerous combinations of these three methodological factors. To address this issue, we performed a split-half analysis by dividing the 143 subjects in Data set 1 into two subgroups matched for age, gender, and mean FD, between which no significant differences were expected. Then, we investigated the between-group differences using a general linear model with age, gender and mean FD included as covariates. Effect sizes of the significant differences were also assessed in terms of Cohen's  $d$  value (Cohen, 1988).

## 3 | RESULTS

Using two R-fMRI data sets (Data set 1 and Data set 2), we generated individual functional networks and then analyzed the small-world properties of the functional networks using different analysis

strategies. Here, we mainly report the results of the binary functional networks with a network density of 15%.

### 3.1 | Three factors affecting individual functional network metrics

Individual functional brain networks constructed using 42 different strategies consistently exhibited small-world topology ( $\sigma > 1$ ) accompanied by high local clustering ( $\gamma > 1$ ) and short path length ( $\lambda \approx 1$ ) for the healthy young adults, HCs, and AD patients. For the healthy young adults in Data set 1, the functional networks exhibited significant differences in all six global properties across the different analysis strategies (i.e., GSR strategies, parcellation schemes, and null network models) via rmANOVA analysis (Table 2). Specifically, regarding the null network-independent properties (i.e.,  $C_p$ ,  $L_p$ , and  $Q$ ), two-way rmANOVA revealed significant effects of two main factors, that is, GSR and parcellation scheme, as well as their interaction (all  $ps < .001$ , Bonferroni corrected). For the null network-dependent properties (i.e.,  $\gamma$ ,  $\lambda$ , and  $\sigma$ ), three-way rmANOVA revealed significant effects of three main factors, that is, GSR strategy, parcellation scheme, and null network model, as well as the interactions between any two of the factors and between all three factors (all  $ps < .001$ , Bonferroni corrected). Similar rmANOVA results were obtained for the HC group and AD patients in Data set 2, with the exception of nonsignificant main effects of GSR on  $\gamma$  in the HC group and on  $Q$  in the AD patients (Supporting Information Tables S2 and S3).

### 3.2 | Convergent and divergent individual differences in functional network organization underlying different analysis strategies

We further assessed whether different analysis strategies affected individual differences in small-world properties and modularity. For the healthy young adults in Data set 1, Figure 2 displays the strategy-to-strategy similarity matrices for all small-world related metrics and modularity and the corresponding dendrograms obtained from the hierarchical cluster analysis. In each dendrogram, strategies in the same cluster were more similar in individual difference profiles than

those in different clusters. For  $C_p$  and  $L_p$ , seven strategies with GSR were grouped into a large cluster. For the metric of  $Q$ , the 14 analysis strategies were largely divided into two clusters with and without GSR at the highest hierarchical level with an exception of one strategy with GSR that was grouped into the family without GSR. These results indicated that GSR, rather than the parcellation schemes, exerted the predominant influence on the inter-subject differences in these three parameters. However, for the metric  $\gamma$ , 42 strategies were mainly grouped into multiple clusters that exhibited the same combination of GSR strategy with the null network models, which indicated a joint influence of the GSR strategy and null network model. For the metric  $\lambda$ , 42 strategies were largely divided into two clusters with and without GSR at the highest hierarchical level, with the exception of four strategies without GSR being grouped into the cluster with GSR, which implies the dominant influence of GSR strategy. For the metric  $\sigma$ , 42 analysis strategies were mainly divided into several clusters that exhibited the same combination of GSR with null network model or parcellation scheme. For the HC group and the AD patients in Data set 2, the strategy-to-strategy similarity matrices and the corresponding hierarchical dendrograms (Figures 3 and 4) were similar to those in the healthy young adults.

### 3.3 | Analysis strategies affecting between-group differences in global functional network organization

In Data set 2, there were no significant differences ( $p > .05$ ) in age, gender, or years of education between the AD patients and HCs (Table 1). The AD patients had an average of 0.26 mm of mean FD (range = 0.11–0.55 mm,  $SD = 0.11$  mm), and the HC group had an average of 0.23 mm of mean FD (range = 0.06–0.73 mm,  $SD = 0.16$  mm). These two groups exhibited no significant difference in mean FD values ( $p = .68$ ). In addition, the two groups showed no significant differences ( $p > .05$ ) in overall functional connectivity under each of the 14 analysis strategies (i.e., 2 GSR strategies  $\times$  7 parcellation schemes; Supporting Information Table S4). We then assessed the potential influence of different analysis strategies on between-group differences in global network properties between the AD and HC groups (Figure 5). We found no significant between-group differences

**TABLE 2** Repeated measures ANOVA results for five small-world parameters and modularity in the healthy young adult group (Data set 1, network density = 15%)

Effect	df	$C_p$		$L_p$		$Q$		$\gamma$		$\lambda$		$\sigma$	
		F	p	F	p	F	p	F	p	F	p	F	p
Parcellation	(6, 852)	342.8	***	237.9	***	1,278.9	***	548.2	***	1,154.3	***	208.8	***
GSR	(1, 142)	33.3	***	167.0	***	44.3	***	163.3	***	55.6	***	207.9	***
Null network model	(2, 284)	N/A	N/A	N/A	N/A	N/A	N/A	3,089.6	***	107.1	***	2,950.9	***
Parcellation $\times$ GSR	(6, 852)	51.4	***	24.9	***	25.9	***	147.5	***	38.3	***	137.9	***
Parcellation $\times$ null network model	(12, 1704)	N/A	N/A	N/A	N/A	N/A	N/A	129.9	***	70.6	***	134.5	***
GSR $\times$ null network model	(2, 284)	N/A	N/A	N/A	N/A	N/A	N/A	177.8	***	23.0	***	147.0	***
Parcellation $\times$ GSR $\times$ null network model	(12, 1704)	N/A	N/A	N/A	N/A	N/A	N/A	34.4	***	14.3	***	30.5	***

Individual functional networks were generated with a fixed-network density of 15%. Two-way rmANOVA was performed on the null network-independent metrics  $C_p$ ,  $L_p$ , and  $Q$  with the two main factors of parcellation and GSR. Three-way rmANOVA was performed on the null network-dependent metrics  $\gamma$ ,  $\lambda$ , and  $\sigma$  with three main factors of parcellation, GSR and null network model. GSR = global signal regression; N/A = not applicable.

\*\*\* $p < .001$ , Bonferroni corrected.

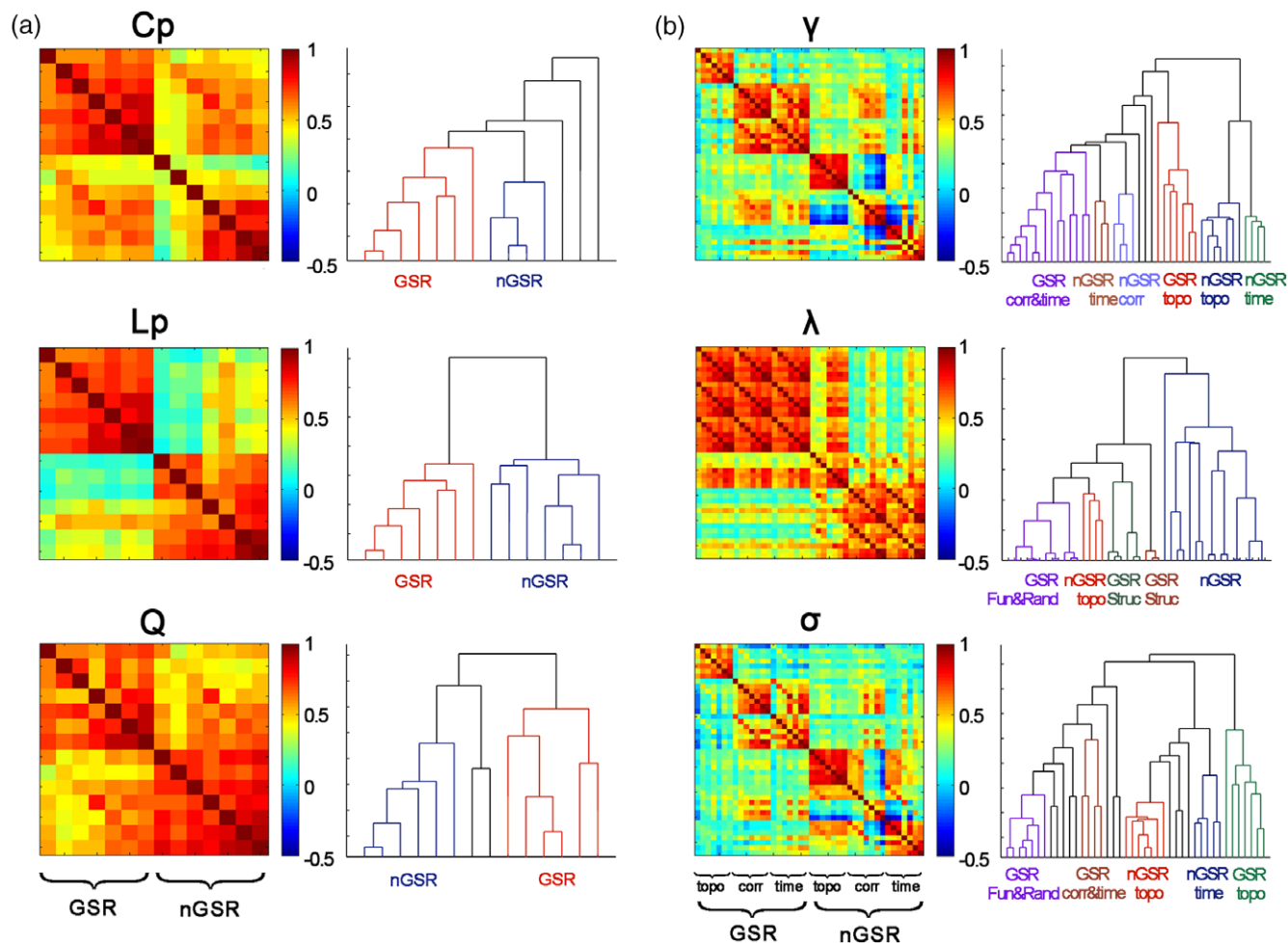


**FIGURE 2** Strategy-to-strategy similarity matrices for individual differences in five small-world parameters (i.e.,  $C_p$ ,  $L_p$ ,  $\gamma$ ,  $\lambda$ , and  $\sigma$ ) and modularity ( $Q$ ) and the corresponding dendrograms obtained from the hierarchical cluster analyses for the healthy young adult group at the network density of 15% (Data set 1). (a) Strategy-to-strategy ( $14 \times 14$ ) similarity matrices (i.e., 2 GSR strategies  $\times$  7 parcellation schemes) and the corresponding dendrograms for  $C_p$ ,  $L_p$ , and  $Q$ . (b) strategy-to-strategy ( $42 \times 42$ ) similarity matrices (i.e., 2 GSR strategies  $\times$  7 parcellation schemes  $\times$  3 null network models) and the corresponding dendrograms for  $\gamma$ ,  $\lambda$ , and  $\sigma$ . Characters under each dendrogram denote the dominate factors affecting the clustering analysis. GSR = global signal regression (i.e., with GSR); nGSR = no global signal regression (i.e., without GSR); topo = topological randomization; corr = correlation matrix randomization; time = time series randomization; fun = functionally defined parcellation; Struc = structurally defined parcellation; Rand = Random-1024 parcellation [Color figure can be viewed at [wileyonlinelibrary.com](http://wileyonlinelibrary.com)]

in the condition of GSR even without correction for multiple comparisons (all  $p$ s  $>$  .05, uncorrected). In contrast, in the condition of without GSR, significantly lower values of  $\gamma$  and  $\sigma$  with medium to large effect sizes were observed in the AD patients when compared with the HC group under the conditions of Craddock-200 and Random-1024 with topological randomization (all  $p$ s  $<$  .05, Bonferroni corrected). Additional differences with small to medium effect sizes were observed in other conditions of without GSR when multiple comparison corrections were not performed. Significantly lower values of  $\gamma$  and  $\sigma$  were observed in the AD group under the conditions of Dosenbach-160 and Power-264 with topological randomization ( $p$ s  $<$  .05, uncorrected). Significantly lower values of  $Q$  were also observed in the AD group for five parcellation schemes without GSR ( $p$ s  $<$  .05, uncorrected), including AAL-90, Dosenbach-160, Craddock-200, Power-264, and Random-1024. In addition, for AAL-90, the metrics of  $L_p$  and  $\lambda$  in AD patients showed significantly higher values than those of the

HC group with correlation randomization and time series randomization ( $p$ s  $<$  .05, uncorrected).

### 3.4 | Whole-brain functional hubs and between-group differences in nodal degree centrality

We detected hub regions within the HC group and within the AD patients via the metric of nodal degree centrality under each of the 14 analysis strategies (GSR or not  $\times$  7 parcellation schemes). Figure 6a showed the occurrence probability maps as hubs across seven parcellations in the conditions of with and without GSR, separately. With GSR (Figure 6a, left), consistent functional hubs (i.e., probability  $>$  0.5) in the HC group were mainly located at the posterior cingulate gyrus/precuneus, angular gyrus, supramarginal gyrus, inferior frontal gyrus, insula, left midcingulate cortex, and right supplementary motor area. The spatial distributions of consistent hub regions (i.e., probability  $>$  0.5) in the

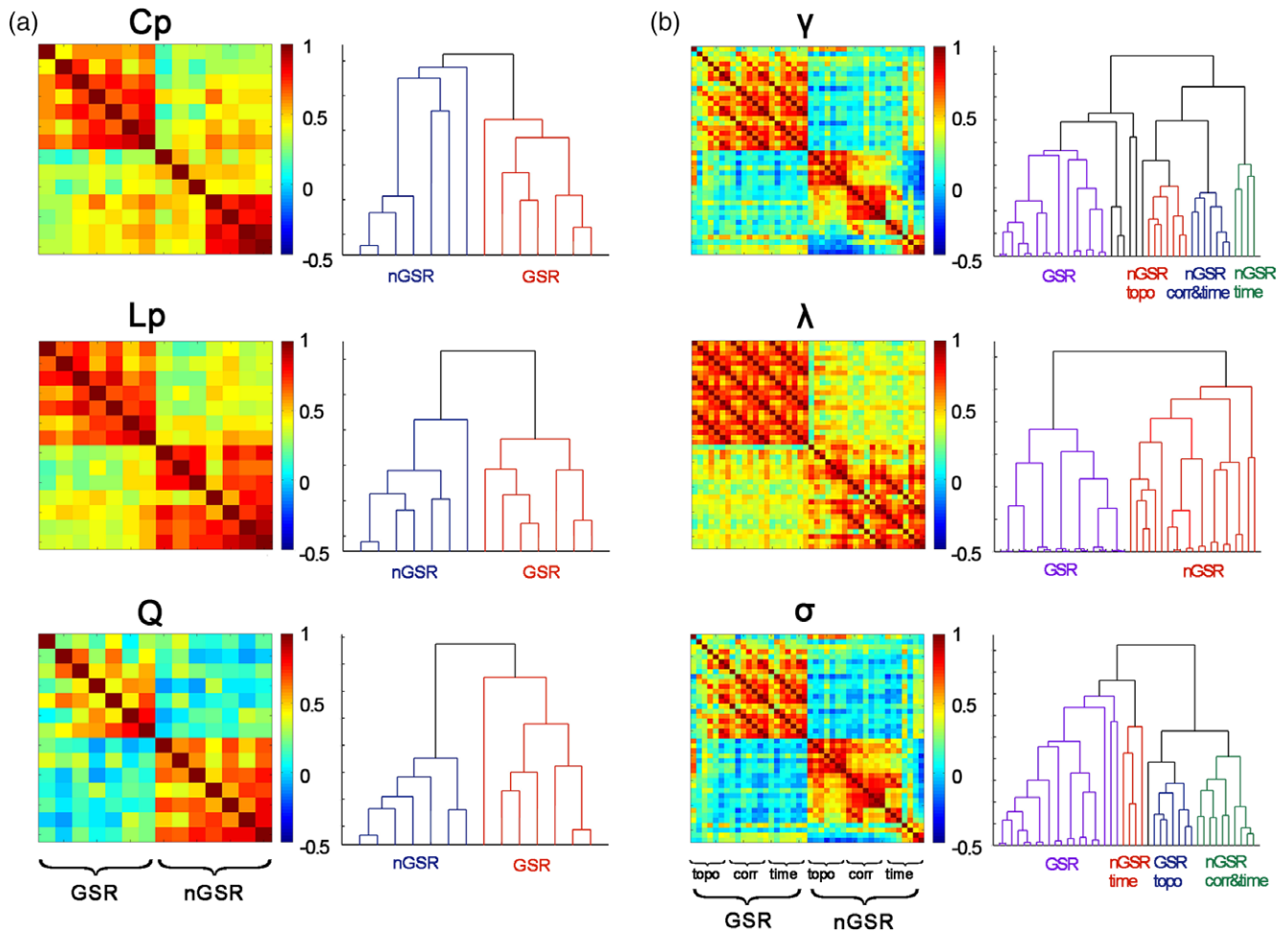


**FIGURE 3** Strategy-to-strategy similarity matrices for individual differences in five small-world parameters (i.e.,  $C_p$ ,  $L_p$ ,  $\gamma$ ,  $\lambda$ , and  $\sigma$ ) and modularity ( $Q$ ) and the corresponding dendrograms obtained from the hierarchical cluster analyses for the HC group at the network density of 15% (Data set 2). (a) Strategy-to-strategy ( $14 \times 14$ ) similarity matrices (i.e., 2 GSR strategies  $\times$  7 parcellation schemes) and the corresponding dendrograms for  $C_p$ ,  $L_p$ , and  $Q$ . (b) strategy-to-strategy ( $42 \times 42$ ) similarity matrices (i.e., 2 GSR strategies  $\times$  7 parcellation schemes  $\times$  3 null network models) and the corresponding dendrograms for  $\gamma$ ,  $\lambda$ , and  $\sigma$ . Characters under each dendrogram denote the dominate factors affecting the clustering analysis. GSR = global signal regression (i.e., with GSR); nGSR = no global signal regression (i.e., without GSR); topo = topological randomization; corr = correlation matrix randomization; time = time series randomization [Color figure can be viewed at [wileyonlinelibrary.com](http://wileyonlinelibrary.com)]

AD group were similar to those in the HC group via visual inspection with the exception of additional consistent hubs at the middle frontal gyrus and medial prefrontal cortex. Notably, spatial patterns of consistent functional hubs obtained without GSR (Figure 6a, right) were different from those obtained with GSR (Figure 6a, left). Specifically, in the HC group, several regions of precuneus, inferior frontal cortex, and supramarginal gyrus became inconspicuous, and additional consistent hubs were observed at the primary areas (e.g., pre/postcentral gyrus, occipital cortex, and superior temporal gyrus). The locations of consistent hub regions in the AD patients were similar to those in the HCs with the primary exceptions at the superior frontal gyrus and medial prefrontal cortex. To further quantify the influence of GSR strategies, we obtained the spatial similarity of the group-level nodal degree maps between two conditions of GSR or not under each parcellation (Supporting Information Table S5). Significant correlations were observed for all parcellations (all  $p_s < .01$ ) regardless of the HC or AD groups considered, with the exception of AAL-90 ( $p > .05$ ). The

correlation values ranged from 0.08 to 0.78 across seven parcellation schemes, which indicated a remarkable influence of GSR strategy on the spatial patterns of degree centrality in a parcellation-dependent way.

Compared with the HC group, the AD patients exhibited significantly decreased degree values (all  $p_s < 1/N$ ,  $N$ , ROI number of each parcellation) but with low spatial overlap across seven parcellation schemes (Figure 6b). With GSR, significant differences were mainly located at the posterior cingulate gyrus, angular gyrus, supramarginal gyrus, inferior frontal gyrus, insula, and midcingulate cortex, as well as the precentral gyrus and the right middle temporal gyrus; most of these regions were identified as consistent hub regions in the HC group. Compatible with GSR, the regions that exhibited significant differences in the condition of without GSR were predominantly located at the consistent hub regions in the HC group (e.g., posterior cingulate cortex, insula, midcingulate cortex, and pre/postcentral gyrus) with the exception of the right middle frontal gyrus.

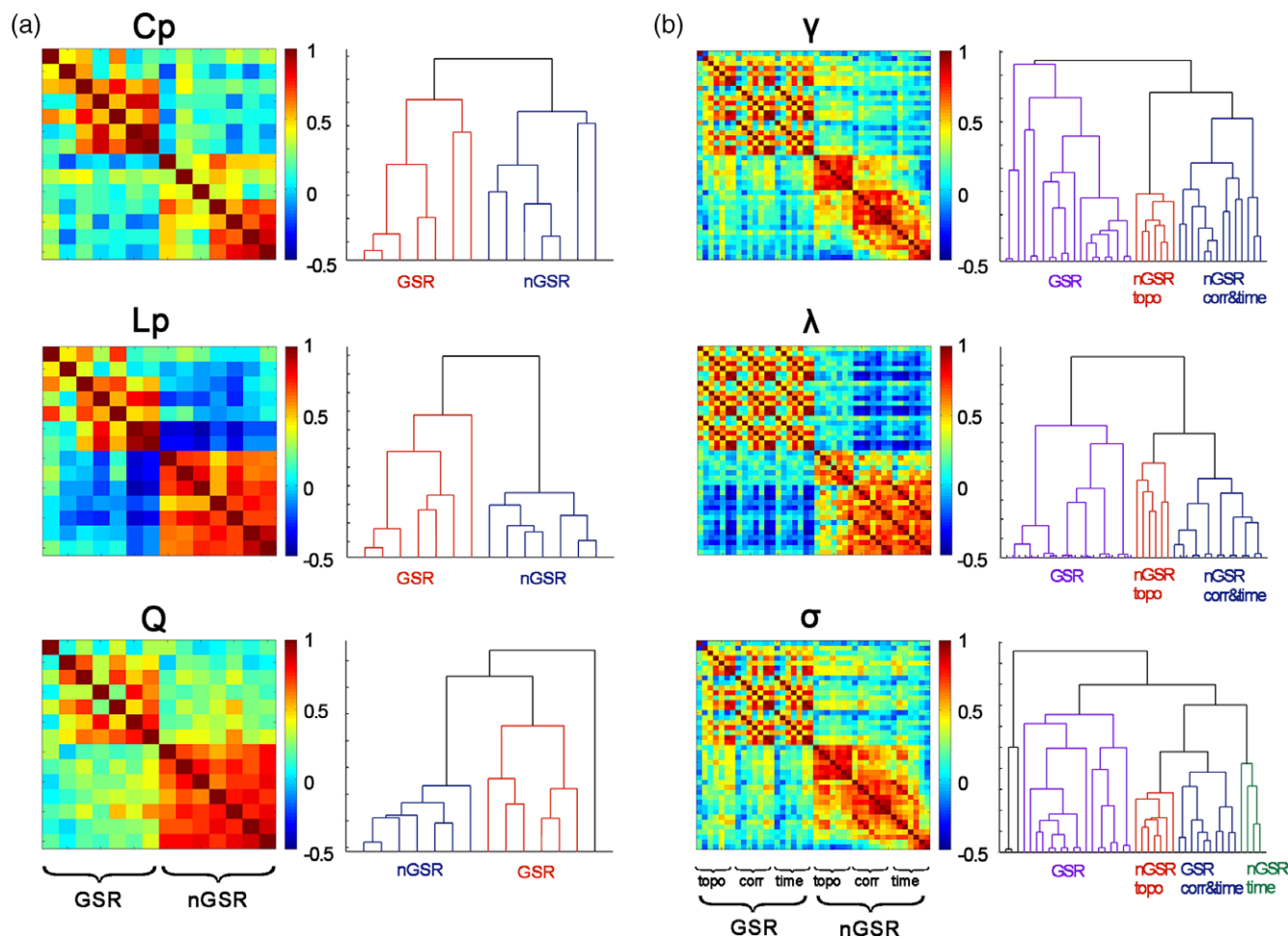


**FIGURE 4** Strategy-to-strategy similarity matrices for individual differences in five small-world parameters (i.e.,  $C_p$ ,  $L_p$ ,  $\gamma$ ,  $\lambda$ , and  $\sigma$ ) and modularity (Q) and the corresponding dendrogram obtained from the hierarchical cluster analyses for the AD patients at the network density of 15% (Data set 2). (a) Strategy-to-strategy ( $14 \times 14$ ) similarity matrices (i.e., 2 GSR strategies  $\times$  7 parcellation schemes) and the corresponding dendrograms for  $C_p$ ,  $L_p$ , and Q. (b) strategy-to-strategy ( $42 \times 42$ ) similarity matrices (i.e., 2 GSR strategies  $\times$  7 parcellation schemes  $\times$  3 null network models) and the corresponding dendrograms for  $\gamma$ ,  $\lambda$ , and  $\sigma$ . Characters under each dendrogram denote the dominate factors affecting the clustering analysis. GSR = global signal regression (i.e., with GSR); nGSR = no global signal regression (i.e., without GSR); topo = topological randomization; corr = correlation matrix randomization; time = time series randomization [Color figure can be viewed at [wileyonlinelibrary.com](http://wileyonlinelibrary.com)]

### 3.5 | Influence on individual differences and between-group comparisons in functional networks constructed with a fixed correlation threshold

In addition to the fixed-density thresholding approach, individual binary functional networks were also generated for subjects in both Data set 1 and Data set 2 using a fixed-correlation threshold with  $r = .2$ . Most of the results were compatible with the previous main findings (Table 3, Figures 7 and 8), including the significant influence on the estimations and individual differences of global network metrics, as well as the between-group comparison in nodal degree centrality. Of note, in the hierarchical cluster analysis for healthy young adults in Data set 1, the influence of several strategies became more conspicuous, including the effects of the GSR strategy on  $C_p$ ,  $L_p$ , and Q and the effects of the null network model on  $\gamma$ ,  $\lambda$ , and  $\sigma$ . Similar effects were also observed for the HC group and the AD patients in Data set 2 (Supporting Information Figures S2 and S3), suggesting the dominant influence of GSR strategy and null network model on the individual variability profiles in small-

world related metrics and modularity. When detecting the between-group differences (AD vs. HC) in Data set 2, we found that the density of individual functional networks varied across individuals and across 14 analysis strategies (GSR or not  $\times$  7 parcellation schemes) (range of group-averaged density: AD, 0.110–0.161 with GSR, 0.336–0.629 with nGSR; HC, 0.107–0.165 with GSR, 0.356–0.653 with nGSR). No significant differences were observed in the network density between two groups under each of the 14 analysis strategies (all  $p$ s  $> .5$ , uncorrected). Different from the fixed-density thresholding approach, no significant difference was observed in any of the global metrics between the AD and HC groups even without correction for multiple comparisons, regardless of the analysis strategy considered (all  $p$ s  $> .5$ , uncorrected).

### 3.6 | Validation results

We assessed the effects of head motion and network construction strategies on our main findings. In addition, we also explored the reliability of the between-group differences (AD vs. HC) in global network

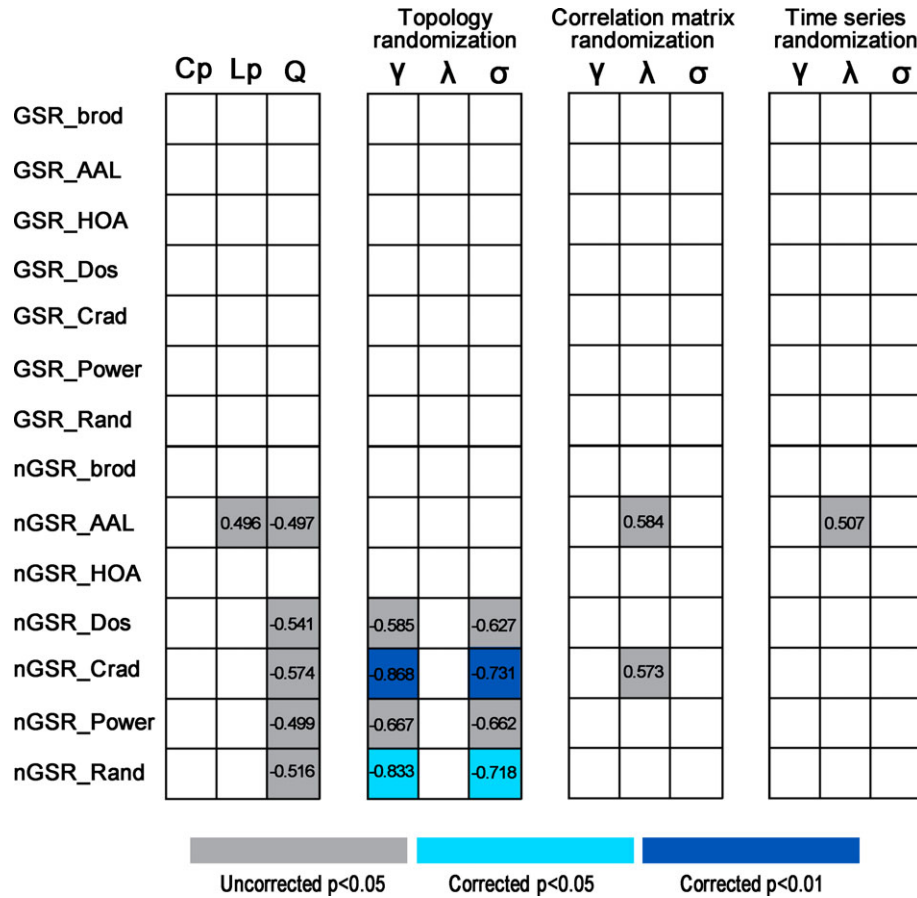


**FIGURE 5** Significant between-group differences (AD vs. HC) under different analysis strategies at the network density of 15% (Data set 2). Significant differences with different  $p$  values are marked by different colors, including uncorrected  $p < .05$ , corrected  $p < .05$ , and corrected  $p < .01$ . Effect sizes of significant group differences are indicated by numbers. HC = healthy control; AD = Alzheimer's disease; GSR = global signal regression (i.e., with GSR); nGSR = no global signal regression (i.e., without GSR); Brod = Brodmann-82 atlas; AAL = AAL-90 parcellation; HOA = HOA-112 parcellation; Dos = Dosenbach-160 parcellation; Crad = Craddock-200 parcellation; Power = Power-264 parcellation; Rand = Random-1024 parcellation; topo = topological randomization; corr = correlation matrix randomization; time = time series randomization [Color figure can be viewed at [wileyonlinelibrary.com](http://wileyonlinelibrary.com)]

metrics. (a) *Effects of head motion*: using partial correlation, the resulting strategy-to-strategy similarity matrices (Supporting Information Figure S4) exhibited spatial patterns that were highly similar to those obtained without controlling for mean FD (Pearson's correlations:  $C_p$ ,  $r = .992$ ;  $L_p$ ,  $r = .993$ ;  $Q$ ,  $r = .986$ ;  $\gamma$ ,  $r = .995$ ;  $\lambda$ ,  $r = .994$ ;  $\sigma$ ,  $r = .995$ ; all  $ps < .0001$ ). In terms of hierarchical clustering, the findings (Supporting Information Figure S4) were highly consistent with the main results (Figure 2). (b) *Effects of network density*: the main findings were almost unchanged for the binary functional networks constructed at other network densities (i.e., 10, 20, and 30%; Supporting Information Tables S6–S8 and Figures S5–S11). (c) *Effects of network type*: most of the main findings were reproducible when considering weighted functional networks (Supporting Information Table S9 and Figures S11–S13). Of note, similar to the fixed-correlation thresholding approach, the influences of the GSR strategy, and the null network model also became more conspicuous in the weighted functional networks, including the effects of GSR strategy on  $C_p$ ,  $L_p$ , and  $Q$  and the effects of the null network model on  $\gamma$ ,  $\lambda$ , and  $\sigma$  (Supporting Information Figure S12). (d) *Reliability of the between-group difference detection*: after applying a split-half approach to 143 healthy young adults in Data set 1, two subgroups of subjects were obtained with 71 subjects in one group and

72 subjects in the other. These two groups exhibited no differences in age, gender, or mean FD (all  $ps > .05$ ). No significant between-group differences were found in any of the six global metrics of interest (all  $ps > .05$ , Bonferroni corrected), with the exception of significant differences under the condition of GSR and AAL-90 in the metric  $L_p$  and  $\lambda$  (i.e., correlation and time series randomization; all  $ps < .05$ , Bonferroni corrected) (Supporting Information Figure S14). These differences between two subgroups of healthy young adults showed small effect sizes, and the network metrics (i.e.,  $L_p$  and  $\lambda$ ) and analysis strategies (i.e., GSR strategies) observed had nothing in common with those between the AD and HC groups. When multiple comparisons were not corrected, significant differences ( $p < .05$  uncorrected) with small effect sizes were only observed in the case of GSR (i.e., in  $Q$ ,  $\gamma$ ,  $\lambda$ , and  $\sigma$ ), except a difference in  $Q$  in the condition of without GSR and Dosenbach-160 (Supporting Information Figure S14).

## 4 | DISCUSSION

This study comprehensively investigated the influence of three factors (i.e., GSR strategy, parcellation scheme, and null network model) on

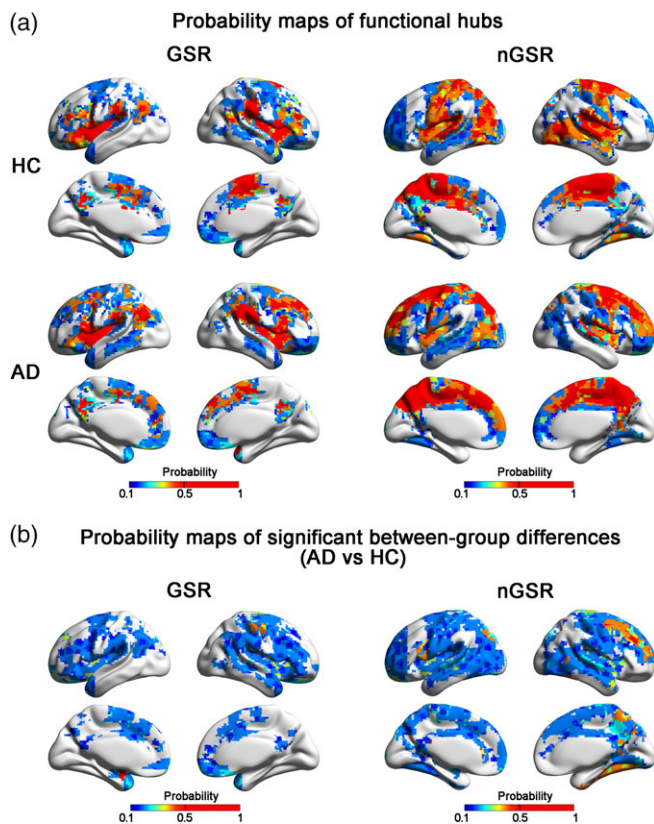


**FIGURE 6** Probability maps of functional hubs and probability maps of significant between-group differences in degree centrality at the network density of 15% (Data set 2). (a) Occurrence probability maps as functional hubs for the HC group and AD patients in the cases of GSR and without GSR. (b) Occurrence probability maps of significant between-group differences in the cases of GSR and without GSR. For each voxel, the occurrence probability as hubs or significant regions under each condition (i.e., with or without GSR) were defined as the number of parcellation schemes under which this voxel was detected as a hub or a significant region divided by the total number of parcellation schemes containing this voxel. In (a,b), brain regions that had occurrence probability below 0.1 (i.e., lower limit of the color bar) are not displayed (i.e., in gray color). The hemispheric surfaces were visualized using BrainNet viewer (Xia, Wang, & He, 2013). GSR = global signal regression (i.e., with GSR); nGSR = no global signal regression (i.e., without GSR); HC = healthy control; AD = Alzheimer's disease [Color figure can be viewed at [wileyonlinelibrary.com](http://wileyonlinelibrary.com)]

aspects of the topological properties of functional networks in healthy adults and AD-related network changes in human brain functional network analyses. First, we found that these three factors not only significantly affected the quantitative values of small-world properties and modularity but also influenced their inter-subject differences. Regarding the latter, the GSR strategy exhibited a predominant influence on most of the properties (i.e.,  $C_p$ ,  $L_p$ ,  $Q$ , and  $\lambda$ ). Second, we found that these three factors influenced the sensitivity of the detection of group differences between the AD patients and the HC group. Notably, the analysis strategies without GSR and topology randomization exhibited higher sensitivities in the detection of between-group differences than the other strategies. Finally, we found that the GSR strategy dominantly influenced the spatial distribution of the hubs and between-group differences in nodal degree. These findings highlight

the joint influence of these three factors on functional network analyses in both healthy and diseased populations, which may be informative for the selection of strategies for data preprocessing and network analysis in future R-fMRI functional network studies.

#### 4.1 | Influence of global signal regression on functional network analysis

Controversy persists regarding whether the global signal should be removed during data preprocessing (Fox, Zhang, Snyder, & Raichle, 2009; Murphy et al., 2009; Murphy & Fox, 2016). One of the main reasons is that the GSR may affect the correlation structure (Murphy et al., 2009) and thus influence the functional network topological properties (Braun et al., 2012; Liang et al., 2012; Liao et al., 2013). Consistent with previous studies, our analysis of two data sets revealed significant effects of GSR on the topological properties of functional networks, including small-world attributes, modularity, and hubs, in healthy young adults, healthy elderly adults, and AD patients. Moreover, we found that GSR strategies influenced the individual differences in topological properties and the sensitivity of the detection of differences between the AD and HC groups. Significant between-group differences were only observed under the strategies without GSR (Figure 5 and Supporting Information Figure S11). It should be noted that the network metrics (i.e.,  $\gamma$  and  $\sigma$ ) and analysis strategies (i.e., without GSR strategies) observed between the AD and HC groups had nothing in common with spurious differences observed between two subsets of healthy young adults (Supporting Information Figure S14). Moreover, these significant differences (AD vs. HC) showed medium to large effect sizes, which were larger than those of spurious differences. Considering the above reasons, we speculate that the significant differences observed between the AD and HC groups are more likely to be meaningful and reliable, rather than simply artifacts introduced by methodological artifacts. Strategies without GSR may be more sensitive in the between-group comparisons (i.e., AD vs. HC) in global network metrics. Similarly, a recent functional network study found that more significant differences in global clustering coefficient and nodal centrality measures were observed between major depression patients and HCs in specific strategies without GSR (Borchardt et al., 2016). All these findings suggest that the global signal may contain subject-specific and disease-related information in both young and elderly subjects. Regression of the global signal during data preprocessing may blur subject-specific information and decrease the sensitivity of between-group difference detection. Interestingly, a recent study reported that GSR reduced the detection sensitivity of abnormalities in the power and variance of gray matter signals in patients with schizophrenia but not in patients with bipolar disorder (Yang et al., 2014), which further indicated that the global signal may be disease-dependent. In our study, the changes in global signal in AD may be attributable to widely distributed gray matter atrophy; however, the underlying mechanism should be further elucidated. Together, these findings suggest that more attention should be paid to GSR in investigations of functional network organization in different diseases.

**TABLE 3** Repeated-measures ANOVA results for five small-world parameters and modularity in the healthy young adult group (Data set 1, correlation threshold = 0.2)

Effect	df	$C_p$		$L_p$		Q		$\gamma$		$\lambda$		$\sigma$	
		F	p	F	p	F	p	F	p	F	p	F	p
Parcellation	(6, 852)	2,860.7	***	2,763.0	***	658.4	***	420.9	***	1,558.5	***	506.0	***
GSR	(1, 142)	919.6	***	2,638.2	***	1980.5	***	3,962.2	***	3,806.8	***	1,210.4	***
Null network model	(2, 284)	N/A	N/A	N/A	N/A	N/A	N/A	2,103.1	***	16,258.8	***	1,071.9	***
Parcellation × GSR	(6, 852)	479.4	***	834.8	***	505.6	***	474.8	***	543.2	***	382.4	***
Parcellation × null network model	(12, 1704)	N/A	N/A	N/A	N/A	N/A	N/A	373.2	***	702.5	***	368.2	***
GSR × null network model	(2, 284)	N/A	N/A	N/A	N/A	N/A	N/A	3,917.5	***	17,445.6	***	1,990.7	***
Parcellation × GSR × null network model	(12, 1704)	N/A	N/A	N/A	N/A	N/A	N/A	440.7	***	875.6	***	439.0	***

Individual functional networks were generated with a fixed-correlation threshold of 0.2. Two-way rmANOVA was performed on the null network-independent metrics  $C_p$ ,  $L_p$ , and Q with the two main factors of parcellation and GSR. Three-way rmANOVA was performed on the null network-dependent metrics  $\gamma$ ,  $\lambda$ , and  $\sigma$  with three main factors of parcellation, GSR, and null network model. GSR = global signal regression; N/A = not applicable. \*\*\* $p < .001$ , Bonferroni corrected.

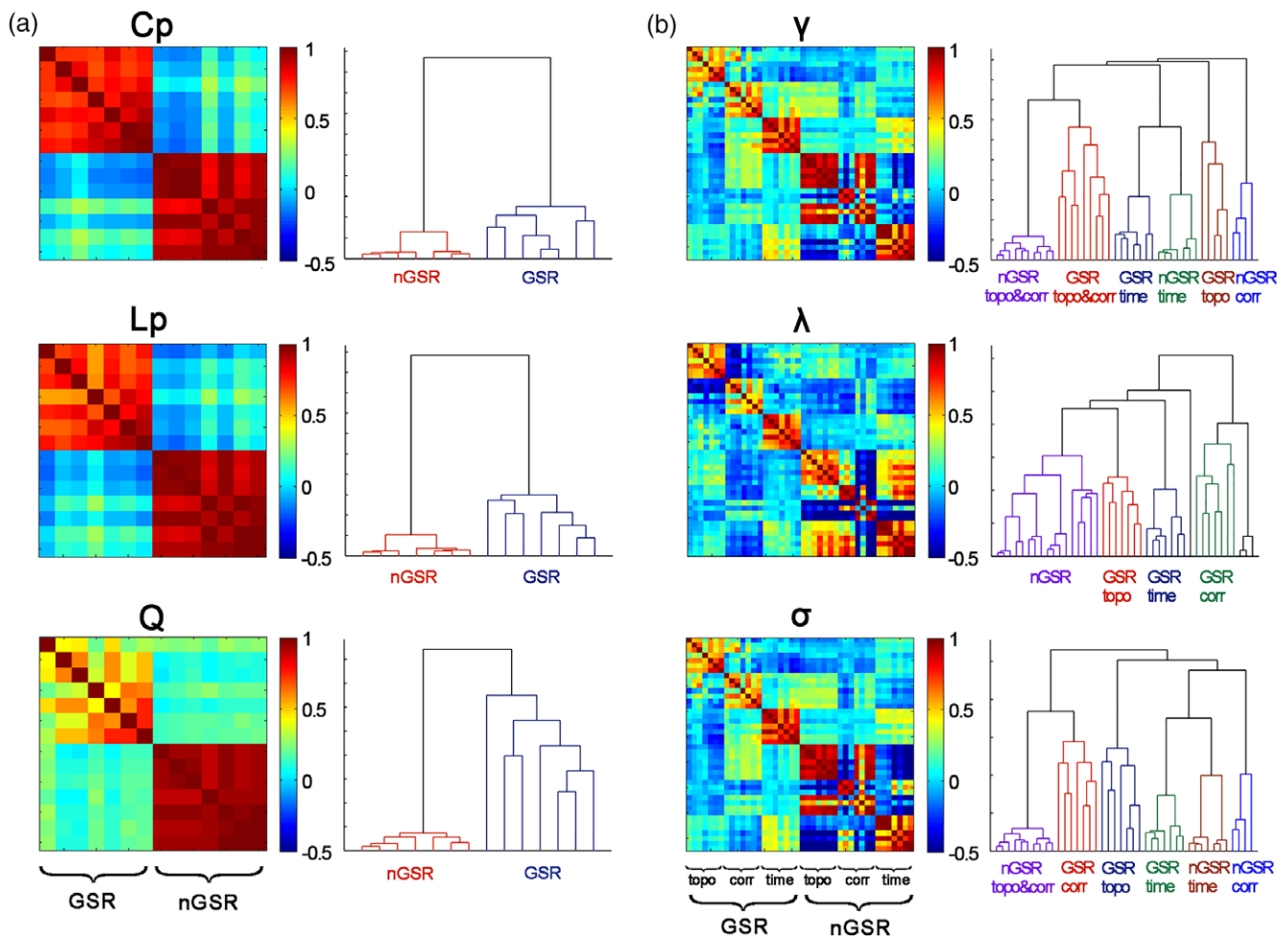


**FIGURE 7** Strategy-to-strategy similarity matrices for individual differences in five small-world parameters (i.e.,  $C_p$ ,  $L_p$ ,  $\gamma$ ,  $\lambda$ , and  $\sigma$ ) and modularity (Q) and the corresponding dendrograms obtained from the hierarchical cluster analyses for the healthy young adult group at the correlation threshold of 0.2 (Data set 1). (a) Strategy-to-strategy ( $14 \times 14$ ) similarity matrices (i.e., 2 GSR strategies  $\times$  7 parcellation schemes) and the corresponding dendrograms for  $C_p$ ,  $L_p$ , and Q. (b) strategy-to-strategy ( $42 \times 42$ ) similarity matrices (i.e., 2 GSR strategies  $\times$  7 parcellation schemes  $\times$  3 null network models) and the corresponding dendrograms for  $\gamma$ ,  $\lambda$ , and  $\sigma$ . Characters under each dendrogram denote the dominate factors affecting the clustering analysis. GSR = global signal regression (i.e., with GSR); nGSR = no global signal regression (i.e., without GSR); topo = topological randomization; corr = correlation matrix randomization; time = time series randomization [Color figure can be viewed at wileyonlinelibrary.com]

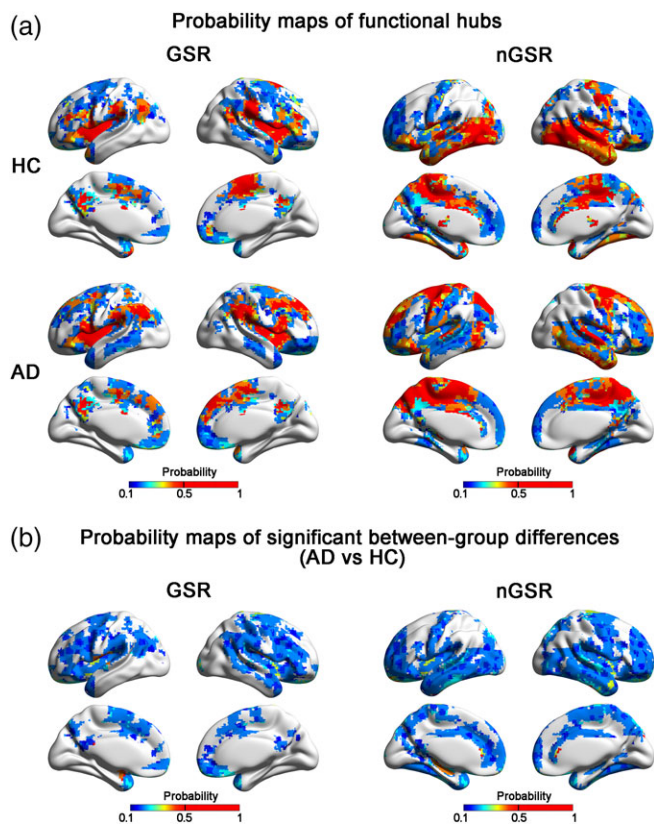


**FIGURE 8** Probability maps of functional hubs and probability maps of significant between-group differences in degree centrality at the correlation threshold of 0.2 (Data set 2). (a) Occurrence probability maps as functional hubs for the HC group and AD patients in the cases of GSR and without GSR. (b) Occurrence probability maps of significant between-group differences in the cases of GSR and without GSR. For each voxel, the occurrence probability as hubs or significant regions under each condition (i.e., with or without GSR) were defined as the number of parcellation schemes under which this voxel was detected as a hub or a significant region divided by the total number of parcellation schemes containing this voxel. In (a,b), brain regions that had occurrence probability below 0.1 (i.e., lower limit of the color bar) are not displayed (i.e., in gray color). The hemispheric surfaces were visualized using BrainNet viewer (Xia et al., 2013). GSR = global signal regression (i.e., with GSR); nGSR = no global signal regression (i.e., without GSR); HC = healthy control; AD = Alzheimer's disease [Color figure can be viewed at [wileyonlinelibrary.com](http://wileyonlinelibrary.com)]

## 4.2 | Influence of parcellation scheme on functional network analysis

In graph-based network analysis, the node definition is an important factor (Fornito et al., 2010; Wang et al., 2009; Wig et al., 2011). We used three different types of parcellation schemes (i.e., anatomically constrained, functionally defined and random parcellation schemes) to comprehensively investigate the influence of node definition on functional network analysis. Consistent with the previous study using two anatomical parcellations (Wang et al., 2009), we found that the parcellation schemes indeed influenced the topological properties of functional networks in both healthy subjects and AD patients (Tables 2 and 3, Supporting Information Tables S2 and S3). Moreover, we found that brain parcellation schemes affected the individual differences in

functional network organization (e.g.,  $\lambda$  and  $\sigma$ ). One possible reason is that these parcellation schemes carry different perspectives of information in the brain (Wig et al., 2011). While anatomical parcellation schemes are identified according to histological cytoarchitecture (e.g., Brodmann-82) or sulcal and gyral boundaries (e.g., AAL-90), functional parcellation schemes aim to ensure the coherence of functional activity (e.g., Dosenbach-160 and Power-264) or functional connectivity (e.g., Craddock-200) within the ROIs. In addition, different parcellation schemes exhibit different spatial resolutions, and parcellation schemes with more fine-grained regions tend to show higher homogeneity in functional signals within ROIs (Wig et al., 2011). Similarly, Fornito et al. (2010) found that individual differences were largely consistent for random parcellations with scales greater than 200 regions, which confirms the substantial influence of the spatial resolution of brain nodes on individual difference characterization.

We also found that different parcellation schemes exhibited different sensitivities in detecting differences between the HC group and AD patients (Figure 5 and Supporting Information Figure S11). At the global level, compared with two other anatomical parcellation schemes (Brodmann-82 and HOA-112), one anatomical (AAL-90), three functional (Dosenbach-160, Craddock-200 and Power-264), and one random (Random-1024) parcellation scheme generally detected more significant between-group differences in the condition of without GSR. The superior performance of these parcellation schemes may be explained by the parcellation type and/or network scales. Functionally defined parcellation may promote the functional homogeneity of voxels within a node and thus provide a more accurate description of regional brain activity (Wig et al., 2011). The superior performance of Random-1024 may be attributable to the higher spatial resolution (i.e., 1,024 nodes), which may also have improved the functional homogeneity of the voxels with a finer definition of nodal regions (Fornito et al., 2010). These findings indicate that functionally defined parcellations or high-spatial-resolution random parcellations may be more appropriate for detecting between-group differences in functional network topological properties. At the nodal level, we found that regions that exhibited significant between-group differences in nodal degree exhibited low spatial overlap across seven parcellation schemes regardless of the GSR strategies considered and were characterized by a low occurrence probability below 0.5 for most of the regions detected (Figures 6 and 8). These discrepancies across parcellation schemes might also be related to the parcellation type and/or network scales as discussed above, and the underlying mechanisms require further investigation.

## 4.3 | Influence of null network models on functional network analysis

We found that three null network models influenced the topological architectures of functional networks. For specific topological properties of  $\gamma$  and  $\sigma$ , we found that in addition to GSR strategy the hierarchical clustering was also affected by the null network model (Figures 2 and 7). Similarly, in a recent structural correlation network study, Hosseini and Kesler (2013) reported that these null network models affected the estimation of small-world parameters and their differences between healthy individuals and survivors of acute

lymphoblastic leukemia. Because these three different null network models were designed to correct the local clustering in real networks in different manners (Zalesky et al., 2012), it is reasonable that they exhibited a dominant influence on the two metrics of  $\gamma$  and  $\sigma$ , the estimations of which involve local clustering. Interestingly, compared with the main results using a fixed-density and binary thresholding approach (Figure 2), the influence of null network models on the hierarchical analyses of  $\gamma$ ,  $\lambda$ , and  $\sigma$  became more conspicuous when using either a fixed-correlation threshold (Figure 7) or a weighted network approach (Supporting Information Figure S12). The findings in the latter two approaches may be attributable to the increased deviation of the null networks from the real functional networks in terms of connection number or strength in a null model-dependent manner. Take time series randomization as an example. Because the randomized time series generally exhibited weak connection strength with each other, the null networks generated with a fixed-correlation approach would show a largely reduced network density compared with that of the original functional networks, and those generated with a weighted network approach exhibited weaker connection strength than did the original networks. In contrast, the null networks generated by topological randomization exhibited the same connection density and connection strength distributions as the original functional networks regardless of the thresholding strategies considered. Therefore, applying a fixed-correlation or a weighted network thresholding approach will promote the deviation between the null networks and the real functional networks in a model-dependent manner and thus might strengthen the effects of null network models.

Furthermore, the null network models affected the sensitivity of the detection of differences between the AD patients and the HC group. In comparison with other two models, the topology randomization model detected more between-group differences in specific small-world properties (i.e.,  $\gamma$  and  $\sigma$ ) for most parcellation schemes in the without-GSR condition (Figure 5 and Supporting Information Figure S11). The weak sensitivities of the correlation and time series randomization models may be attributed to the rules for null model generation (Zalesky et al., 2012). The null correlation matrices were generated to have the same correlation distributions as the original matrices, which might have preserved lots of information from the original matrices and thus obscured individual-specific information and AD-related changes. During time series randomization, we randomized the phase of the original time series for each node independently and then generated null networks. This procedure largely reduced the potential coherence between different nodes and may have introduced large random noises that would have hindered the detection of between-group differences. These hypotheses require additional evidence from future work and should be validated in more diseases.

#### 4.4 | Influence of thresholding strategies on functional network analysis

During the functional network construction, a thresholding approach is usually applied to the functional correlation matrix to exclude weak or spurious connections that are potentially introduced by noises. Two commonly used thresholding strategies were employed here,

including a fixed-density thresholding and a fixed-correlation thresholding. These two approaches characterize the relative and absolute network topology of functional organization separately and thus may produce divergent results in contrastive research. Here, we observed significant between-group differences (AD vs. HC) in several global metrics (i.e.,  $\gamma$ ,  $\sigma$ , and  $Q$ ) over a wide range of density values (i.e., 10, 15, 20, and 30%) (Figure 5 and Supporting Information Figure S11) but did not do so with a fixed-correlation threshold ( $r = .2$ ) regardless of the analysis strategies considered. Because the AD and HC groups in this study exhibited no significant differences in overall functional connectivity (Supporting Information Table S4), the vanished between-group differences in the latter case may be related to the different numbers of edges across individual functional networks that result from the application of a fixed-correlation threshold. A previous study demonstrated that network density remarkably affects the estimation of graph metrics (van Wijk, Stam, & Daffertshofer, 2010). Thus, the varying densities across individual networks might increase the inter-individual differences (e.g.,  $SDs$ ) of topological properties within each group and reduce the sensitivity of between-group comparisons of global metrics. Our finding suggests that applying a fixed-density thresholding strategy during functional network construction may confound the between-group comparison in contrastive research, which is compatible with the idea presented by van den Heuvel et al. (2017). Nevertheless, when using a fixed-density thresholding, we should notice that the between-group comparisons of global topological properties (e.g., local clustering) may be biased by the potential between-group differences in the overall functional connectivity (van den Heuvel et al., 2017). In our main analyses, the AD patients and the HC group exhibited no significant differences in the overall functional connectivity, thus the potential influence of the overall functional connectivity can be ignored. In general, the conceptual differences of these two thresholding strategies should be kept in mind in future functional network analysis, especially in contrastive research.

#### 4.5 | Functional network alterations in AD patients

The topological properties (i.e.,  $\gamma$ ,  $\sigma$ , and  $Q$ ) were significantly lower in AD patients when compared with those in HCs, indicating that the functional networks of AD patients exhibited a trend toward a more random configuration with the loss of local information integration and small-world properties. Our findings are consistent with previous fMRI studies (Sanz-Arigita et al., 2010; Supekar et al., 2008), which also revealed a randomization trend in AD patients, and further confirms the disruption of global functional organization in AD patients. Notably, in contrast to our findings, several studies (Liu et al., 2012, 2014; Zhao et al., 2012) have found that the functional networks of AD patients exhibit a trend toward a regular configuration. These discrepant conclusions may be attributed to the heterogeneity of the different AD populations studied (e.g., populations involved different preclinical and clinical stages) and/or differences in network analysis strategies, such as preprocessing procedures, parcellation schemes, and network thresholding strategies (Dai & He, 2014).

Using the measure of degree centrality, we identified functional hubs that were highly connected. With GSR, several regions in the

default-mode network (e.g., posterior cingulate gyrus/precuneus and angular gyrus), supramarginal gyrus, and insula were identified as consistent hubs across parcellations regardless of the HC group or AD group considered. The spatial distribution of hubs was in line with that of previous studies in either health (Buckner et al., 2009; Cocchi et al., 2015; Liang et al., 2013) or disease (Dai et al., 2015). Consistent with previous findings (Du et al., 2015; Liao et al., 2013), we found that the spatial patterns of consistent functional hubs slightly changed in the case of without GSR wherein primary sensorimotor, visual, and auditory areas became more conspicuous. These findings may be attributable to the region-dependent influence of GSR on correlation structure (Liao et al., 2013; Sepulcre et al., 2010). Notably, the spatial pattern of functional hubs is also dependent on the nodal centrality metric considered. A recent study (Power, Schlaggar, et al., 2013) employed a metric of participation coefficient, instead of degree centrality, to identify nodes that played crucial roles in between-community communication and reported a dissimilar spatial pattern of hubs (e.g., lateral frontal cortex). Moreover, we found that GSR affected group differences in nodal degree between AD patients and HCs, and these effects were consistent across different network thresholding approaches, which further suggest that the global signal may contain AD-related information as discussed above. Importantly, in both the with and without GSR conditions, several consistent hub regions (e.g., posterior cingulate cortex/precuneus, left angular gyrus, and insula) in the HC group were found to exhibit significant between-group differences under at least one parcellation scheme, suggesting that hub regions might be preferentially attacked in AD. This finding is consistent with several previous studies (Buckner et al., 2009; Crossley et al., 2014; Dai et al., 2015) and may be explained from two perspectives. On the one hand, Buckner et al. (2009) found that the spatial pattern of hub regions in healthy young subjects overlaps substantially with the A $\beta$  deposition pattern in AD, which may have resulted from the high metabolism of hub regions (Liang et al., 2013; Tomasi et al., 2013). A $\beta$  proteins have toxic effects on neurons and synapses (Selkoe, 2008); therefore, the high A $\beta$  deposition in hub regions could affect the neural activity and thus disrupt their functional connectivity. On the other hand, the hub regions are crucial for information communication, and their disruption may introduce severe abnormalities in functional organization and thus manifest as a brain disorders (Crossley et al., 2014). The mechanism underlying hub alterations in AD patients requires further elucidation. Notably, although the differences in nodal degree centrality were reliable across different network construction approaches, they did not survive Bonferroni or false discovery rate correction. These results should only be considered as a preliminary exploration. A large sample of AD patients should be employed in the future to increase the statistical power.

#### 4.6 | Methodological issues

Several issues should be further considered in the future. First, in this study, we performed the functional network analysis only at the regional level based on different parcellation schemes. As there is no widely accepted gold standard for how to select the parcellation scheme (Arslan et al., 2017), voxel-wise functional network analysis is

an appropriate candidate for future studies due to recent improvements in computing platforms (Du et al., 2018; Wang et al., 2013). The voxel-based functional network analysis may reveal more detailed connectivity information at a higher spatial resolution and reduce the potential bias of regional parcellations. Second, we found that the GSR strategy affected the functional network analyses in both health and diseases. The reason for this effect remains unclear. Because the main purpose of GSR during data preprocessing is to remove the effects of nonneural noise, future studies may employ other strategies, such as regression of the respiration and cardiac signals obtained from a multiconductor, to reduce the influence of nonneural signals while simultaneously avoiding the byproducts of GSR. Third, to reduce the influence of head motion, we first included 24 head motion parameters in the nuisance regression in data preprocessing (Friston et al., 1996; Yan, Cheung, et al., 2013). Then, we validated the results regarding individual differences in healthy young adults (Data set 1) and detected between-group differences (AD vs. HC, Data set 2) by including mean FD values as covariates. However, it is worth mentioning that the effects of head motion may still exist, and this issue requires further investigation involving improving the head motion correction strategies. Finally, in this study, we used AD as an example to investigate the influence of three factors on the whole-brain functional network analyses. However, whether and how the findings of this work can be generalized to other diseases (e.g., Parkinson's disease and depression) requires further investigation.

## 5 | CONCLUSION AND RECOMMENDATIONS

We demonstrated a remarkable joint influence of the GSR strategy, regional parcellation scheme, and null network model on functional network analyses in both health and diseases. Most of the findings were reproducible across different network construction strategies. We make the following recommendations for future human brain functional network studies. First, regarding GSR strategy, we found that GSR strategy greatly affected the sensitivity of the detection of group differences in small-world related metrics and modularity between the AD and HC groups. However, whether and how GSR strategy affects functional network analyses in other diseases (e.g., Parkinson's disease and depression) remains unclear. Because different GSR strategies may provide complementary information about the functional organization of the brain (Murphy & Fox, 2016), we recommend employing both strategies (i.e., GSR or not) during data preprocessing in contrastive research to obtain comprehensive insights. Second, regarding node definition, during the between-group comparison (AD vs. HC) in global metrics, we found that functionally defined parcellations or high-spatial-resolution random parcellations are likely to outperform the structurally defined ones. The reason could be due to that these functional, high-resolution defined nodes better capture functionally meaningful brain units. We believe that these parcellations may be more suitable in future studies aiming to compare functional network topological properties. Third, regarding the null network model, it has been argued that the model of topological randomization does not take into account of inherent transitive

structure of correlation networks (Zalesky et al., 2012). Nevertheless, in our study, the topological randomization model exhibited higher sensitivity in the detection of between-group differences in the absence of GSR compared with the other two null models. Based on the current results, we speculate that the other two models might be conservative (i.e., correlation randomization model) or introduce much noise (i.e., time series randomization model), and that the topological randomization model might be more valuable. Finally, we found that the GSR strategy, parcellation scheme, and null network model jointly affected human brain functional network analyses including the quantitative values of topological properties and their individual difference profiles. Therefore, these three factors should be carefully considered when exploring the brain network mechanisms underlying individual cognitive behaviors and lifespan developments in the future. We hope these recommendations and considerations will be informative in the choices of analysis strategies in future functional network studies.

## ACKNOWLEDGMENTS

This study was supported by the Natural Science Foundation of China (Grant Nos. 91432115, 81620108016, and 81571648), Changjiang Scholar Professorship Award (Award No. T2015027), Beijing Municipal Science & Technology Commission (Grant Nos. Z161100004916027, Z151100003915082, and Z16110000216152), and the Fundamental Research Funds for the Central Universities (Grant Nos. 2015KJJC13, and 2017XTCX04).

## ORCID

Xuhong Liao  <http://orcid.org/0000-0001-6522-0950>

## REFERENCES

- Alavash, M., Doebler, P., Holling, H., Thiel, C. M., & Giessing, C. (2015). Is functional integration of resting state brain networks an unspecific biomarker for working memory performance? *NeuroImage*, *108*, 182–193.
- Arslan, S., Ktena, S. I., Makropoulos, A., Robinson, E. C., Rueckert, D., & Parisot, S. (2017). Human brain mapping: A systematic comparison of parcellation methods for the human cerebral cortex. *NeuroImage*, *13*, 30302–30306.
- Ashburner, J., & Friston, K. J. (2005). Unified segmentation. *NeuroImage*, *26*, 839–851.
- Bassett, D. S., Meyer-Lindenberg, A., Achard, S., Duke, T., & Bullmore, E. (2006). Adaptive reconfiguration of fractal small-world human brain functional networks. *Proceedings of the National Academy of Sciences of the United States of America*, *103*, 19518–19523.
- Birn, R. M., Diamond, J. B., Smith, M. A., & Bandettini, P. A. (2006). Separating respiratory-variation-related fluctuations from neuronal-activity-related fluctuations in fMRI. *NeuroImage*, *31*, 1536–1548.
- Biswal, B., Zerrin Yetkin, F., Haughton, V. M., & Hyde, J. S. (1995). Functional connectivity in the motor cortex of resting human brain using echo-planar MRI. *Magnetic Resonance in Medicine*, *34*, 537–541.
- Biswal, B. B., Mennes, M., Zuo, X. N., Gohel, S., Kelly, C., Smith, S. M., ... Milham, M. P. (2010). Toward discovery science of human brain function. *Proceedings of the National Academy of Sciences of the United States of America*, *107*, 4734–4739.
- Borchardt, V., Lord, A. R., Li, M., van der Meer, J., Heinze, H. J., Bogerts, B., ... Walter, M. (2016). Preprocessing strategy influences graph-based exploration of altered functional networks in major depression. *Human Brain Mapping*, *37*, 1422–1442.
- Braun, U., Plichta, M. M., Esslinger, C., Sauer, C., Haddad, L., Grimm, O., ... Meyer-Lindenberg, A. (2012). Test-retest reliability of resting-state connectivity network characteristics using fMRI and graph theoretical measures. *NeuroImage*, *59*, 1404–1412.
- Brodmann, K. (1909). *Vergleichende lokalisationslehre der grobhirnrinde*. Leipzig: Barth.
- Buckner, R. L., Sepulcre, J., Talukdar, T., Krienen, F. M., Liu, H., Hedden, T., ... Johnson, K. A. (2009). Cortical hubs revealed by intrinsic functional connectivity: Mapping, assessment of stability, and relation to Alzheimer's disease. *The Journal of Neuroscience*, *29*, 1860–1873.
- Bullmore, E., & Sporns, O. (2009). Complex brain networks: Graph theoretical analysis of structural and functional systems. *Nature Reviews. Neuroscience*, *10*, 186–198.
- Bullmore, E. T., & Bassett, D. S. (2011). Brain graphs: Graphical models of the human brain connectome. *Annual Review of Clinical Psychology*, *7*, 113–140.
- Cao, M., Huang, H., & He, Y. (2017). Developmental connectomics from infancy through early childhood. *Trends in Neurosciences*, *40*, 494–506.
- Cocchi, L., Sale, M. V., Lord, A., Zalesky, A., Breakspear, M., & Mattingley, J. B. (2015). Dissociable effects of local inhibitory and excitatory theta-burst stimulation on large-scale brain dynamics. *Journal of Neurophysiology*, *113*, 3375–3385.
- Cohen, J. (1988). *Statistical power analysis for the behavioral sciences* (2nd ed., pp. 19–74). Mahwah NJ: Lawrence Erlbaum Associates.
- Cohen, J. R., & D'Esposito, M. (2016). The segregation and integration of distinct brain networks and their relationship to cognition. *Journal of Neuroscience*, *36*, 12083–12094.
- Craddock, R. C., James, G. A., Holtzheimer, P. E., 3rd, Hu, X. P., & Mayberg, H. S. (2012). A whole brain fMRI atlas generated via spatially constrained spectral clustering. *Human Brain Mapping*, *33*, 1914–1928.
- Crossley, N. A., Mechelli, A., Scott, J., Carletti, F., Fox, P. T., McGuire, P., & Bullmore, E. T. (2014). The hubs of the human connectome are generally implicated in the anatomy of brain disorders. *Brain*, *137*, 2382–2395.
- Dai, Z., & He, Y. (2014). Disrupted structural and functional brain connectomes in mild cognitive impairment and Alzheimer's disease. *Neuroscience Bulletin*, *30*, 217–232.
- Dai, Z., Yan, C., Li, K., Wang, Z., Wang, J., Cao, M., ... He, Y. (2015). Identifying and mapping connectivity patterns of brain network hubs in Alzheimer's disease. *Cerebral Cortex*, *25*, 3723–3742.
- Dai, Z., Yan, C., Wang, Z., Wang, J., Xia, M., Li, K., & He, Y. (2012). Discriminative analysis of early Alzheimer's disease using multi-modal imaging and multi-level characterization with multi-classifier (M3). *NeuroImage*, *59*, 2187–2195.
- Delbeuck, X., Van der Linden, M., & Collette, F. (2003). Alzheimer's disease as a disconnection syndrome? *Neuropsychology Review*, *13*, 79–92.
- Dosenbach, N. U., Nardos, B., Cohen, A. L., Fair, D. A., Power, J. D., Church, J. A., ... Schlaggar, B. L. (2010). Prediction of individual brain maturity using fMRI. *Science*, *329*, 1358–1361.
- Doucet, G. E., Bassett, D. S., Yao, N., Glahn, D. C., & Frangou, S. (2017). The role of intrinsic brain functional connectivity in vulnerability and resilience to bipolar disorder. *The American Journal of Psychiatry*, *174*, 1214–1222.
- Du, H., Xia, M., Zhao, K., Liao, X., Yang, H., Wang, Y., & He, Y. (2018). PAGANI toolkit: Parallel graph-theoretical analysis package for brain network big data. *Human Brain Mapping*, *39*, 1869–1885.
- Du, H. X., Liao, X. H., Lin, Q. X., Li, G. S., Chi, Y. Z., Liu, X., ... Xia, M. R. (2015). Test-retest reliability of graph metrics in high-resolution functional connectomics: A resting-state functional MRI study. *CNS Neuroscience & Therapeutics*, *21*, 802–816.
- Filippi, M., van den Heuvel, M. P., Fornito, A., He, Y., Hulshoff Pol, H. E., Agosta, F., ... Rocca, M. A. (2013). Assessment of system dysfunction in the brain through MRI-based connectomics. *Lancet Neurology*, *12*, 1189–1199.
- Fornito, A., & Bullmore, E. T. (2015). Connectomics: A new paradigm for understanding brain disease. *European Neuropsychopharmacology*, *25*, 733–748.
- Fornito, A., Zalesky, A., & Bullmore, E. T. (2010). Network scaling effects in graph analytic studies of human resting-state FMRI data. *Frontiers in Systems Neuroscience*, *4*, 22.

- Fox, M. D., & Raichle, M. E. (2007). Spontaneous fluctuations in brain activity observed with functional magnetic resonance imaging. *Nature Reviews. Neuroscience*, 8, 700–711.
- Fox, M. D., Zhang, D., Snyder, A. Z., & Raichle, M. E. (2009). The global signal and observed anticorrelated resting state brain networks. *Journal of Neurophysiology*, 101, 3270–3283.
- Friston, K. J., Williams, S., Howard, R., Frackowiak, R. S., & Turner, R. (1996). Movement-related effects in fMRI time-series. *Magnetic Resonance in Medicine*, 35, 346–355.
- Gong, Q., & He, Y. (2015). Depression, neuroimaging and connectomics: A selective overview. *Biological Psychiatry*, 77, 223–235.
- He, Y., Dagher, A., Chen, Z., Charil, A., Zijdenbos, A., Worsley, K., & Evans, A. (2009). Impaired small-world efficiency in structural cortical networks in multiple sclerosis associated with white matter lesion load. *Brain*, 132, 3366–3379.
- He, Y., & Evans, A. (2010). Graph theoretical modeling of brain connectivity. *Current Opinion in Neurology*, 23, 341–350.
- Hosseini, S. M., & Kesler, S. R. (2013). Influence of choice of null network on small-world parameters of structural correlation networks. *PLoS One*, 8, e67354.
- Humphries, M. D., Gurney, K., & Prescott, T. J. (2006). The brainstem reticular formation is a small-world, not scale-free, network. *Proceedings of the Royal Society B: Biological Sciences*, 273, 503–511.
- Kelly, C., Biswal, B. B., Craddock, R. C., Castellanos, F. X., & Milham, M. P. (2012). Characterizing variation in the functional connectome: Promise and pitfalls. *Trends in Cognitive Sciences*, 16, 181–188.
- Kennedy, D. N., Lange, N., Makris, N., Bates, J., Meyer, J., & Caviness, V. S., Jr. (1998). Gyri of the human neocortex: An MRI-based analysis of volume and variance. *Cerebral Cortex*, 8, 372–384.
- Liang, X., Wang, J., Yan, C., Shu, N., Xu, K., Gong, G., & He, Y. (2012). Effects of different correlation metrics and preprocessing factors on small-world brain functional networks: A resting-state functional MRI study. *PLoS One*, 7, e32766.
- Liang, X., Zou, Q., He, Y., & Yang, Y. (2013). Coupling of functional connectivity and regional cerebral blood flow reveals a physiological basis for network hubs of the human brain. *Proceedings of the National Academy of Sciences of the United States of America*, 110, 1929–1934.
- Liao, X., Vasilakos, A. V., & He, Y. (2017). Small-world human brain networks: Perspectives and challenges. *Neuroscience and Biobehavioral Reviews*, 77, 286–300.
- Liao, X. H., Xia, M. R., Xu, T., Dai, Z. J., Cao, X. Y., Niu, H. J., ... He, Y. (2013). Functional brain hubs and their test-retest reliability: A multi-band resting-state functional MRI study. *NeuroImage*, 83, 969–982.
- Lin, Q., Dai, Z., Xia, M., Han, Z., Huang, R., Gong, G., ... He, Y. (2015). A connectivity-based test-retest Data set of multi-modal magnetic resonance imaging in young healthy adults. *Scientific Data*, 2, 150056.
- Liu, J., Xia, M., Dai, Z., Wang, X., Liao, X., Bi, Y., & He, Y. (2017). Intrinsic brain hub connectivity underlies individual differences in spatial working memory. *Cerebral Cortex*, 27, 5496–5508.
- Liu, Y., Yu, C., Zhang, X., Liu, J., Duan, Y., Alexander-Bloch, A. F., ... Bullmore, E. (2014). Impaired long distance functional connectivity and weighted network architecture in Alzheimer's disease. *Cerebral Cortex*, 24, 1422–1435.
- Liu, Z., Zhang, Y., Yan, H., Bai, L., Dai, R., Wei, W., ... Tian, J. (2012). Altered topological patterns of brain networks in mild cognitive impairment and Alzheimer's disease: A resting-state fMRI study. *Psychiatry Research*, 202, 118–125.
- Lynall, M. E., Bassett, D. S., Kerwin, R., McKenna, P. J., Kitzbichler, M., Muller, U., & Bullmore, E. (2010). Functional connectivity and brain networks in schizophrenia. *The Journal of Neuroscience*, 30, 9477–9487.
- Makris, N., Meyer, J. W., Bates, J. F., Yeterian, E. H., Kennedy, D. N., & Caviness, V. S. (1999). MRI-based topographic parcellation of human cerebral white matter and nuclei II. Rationale and applications with systematics of cerebral connectivity. *NeuroImage*, 9, 18–45.
- Maslov, S., & Sneppen, K. (2002). Specificity and stability in topology of protein networks. *Science*, 296, 910–913.
- McKhann, G., Drachman, D., Folstein, M., Katzman, R., Price, D., & Stadlan, E. M. (1984). Clinical diagnosis of Alzheimer's disease: Report of the NINCDS-ADRDA work group under the auspices of Department of Health and Human Services Task Force on Alzheimer's disease. *Neurology*, 34, 939–944.
- Murphy, K., Birn, R. M., Handwerker, D. A., Jones, T. B., & Bandettini, P. A. (2009). The impact of global signal regression on resting state correlations: Are anti-correlated networks introduced? *NeuroImage*, 44, 893–905.
- Murphy, K., & Fox, M. D. (2016). Towards a consensus regarding global signal regression for resting state functional connectivity MRI. *NeuroImage*, 22, 30671–30671.
- Newman, M. E. (2004). Fast algorithm for detecting community structure in networks. *Physical Review. E, Statistical, Nonlinear, and Soft Matter Physics*, 69, 18.
- Newman, M. E. (2006). Modularity and community structure in networks. *Proceedings of the National Academy of Sciences of the United States of America*, 103, 8577–8582.
- Newman, M. E., & Girvan, M. (2004). Finding and evaluating community structure in networks. *Physical Review. E, Statistical, Nonlinear, and Soft Matter Physics*, 69, 026113.
- Power, J. D., Barnes, K. A., Snyder, A. Z., Schlaggar, B. L., & Petersen, S. E. (2012). Spurious but systematic correlations in functional connectivity MRI networks arise from subject motion. *NeuroImage*, 59, 2142–2154.
- Power, J. D., Cohen, A. L., Nelson, S. M., Wig, G. S., Barnes, K. A., Church, J. A., ... Petersen, S. E. (2011). Functional network organization of the human brain. *Neuron*, 72, 665–678.
- Power, J. D., Mitra, A., Laumann, T. O., Snyder, A. Z., Schlaggar, B. L., & Petersen, S. E. (2013). Methods to detect, characterize, and remove motion artifact in resting state fMRI. *NeuroImage*, 84, 320–341.
- Power, J. D., Plitt, M., Laumann, T. O., & Martin, A. (2016). Sources and implications of whole-brain fMRI signals in humans. *NeuroImage*, 15, 30515–30518.
- Power, J. D., Schlaggar, B. L., Lessov-Schlaggar, C. N., & Petersen, S. E. (2013). Evidence for hubs in human functional brain networks. *Neuron*, 79, 798–813.
- Power, J. D., Schlaggar, B. L., & Petersen, S. E. (2015). Recent progress and outstanding issues in motion correction in resting state fMRI. *NeuroImage*, 105, 536–551.
- Sanz-Arigita, E. J., Schoonheim, M. M., Damoiseaux, J. S., Rombouts, S. A., Maris, E., Barkhof, F., ... Stam, C. J. (2010). Loss of 'small-world' networks in Alzheimer's disease: Graph analysis of FMRI resting-state functional connectivity. *PLoS One*, 5, e13788.
- Satterthwaite, T. D., Elliott, M. A., Gerraty, R. T., Ruparel, K., Loughhead, J., Calkins, M. E., ... Wolf, D. H. (2013). An improved framework for confound regression and filtering for control of motion artifact in the preprocessing of resting-state functional connectivity data. *NeuroImage*, 64, 240–256.
- Sawilowsky, S. S. (2009). New effect size rules of thumb. *Journal of Modern Applied Statistical Methods*, 8, 597–599.
- Scholvinck, M. L., Maier, A., Ye, F. Q., Duyn, J. H., & Leopold, D. A. (2010). Neural basis of global resting-state fMRI activity. *Proceedings of the National Academy of Sciences of the United States of America*, 107, 10238–10243.
- Selkoe, D. J. (2008). Soluble oligomers of the amyloid beta-protein impair synaptic plasticity and behavior. *Behavioural Brain Research*, 192, 106–113.
- Sepulcre, J., Liu, H., Talukdar, T., Martincorena, I., Yeo, B. T., & Buckner, R. L. (2010). The organization of local and distant functional connectivity in the human brain. *PLoS Computational Biology*, 6, e1000808.
- Sokal, R. R. (1958). A statistical method for evaluating systematic relationship. *University of Kansas Science Bulletin*, 28, 1409–1438.
- Stam, C. J. (2014). Modern network science of neurological disorders. *Nature Reviews. Neuroscience*, 15, 683–695.
- Supekar, K., Menon, V., Rubin, D., Musen, M., & Greicius, M. D. (2008). Network analysis of intrinsic functional brain connectivity in Alzheimer's disease. *PLoS Computational Biology*, 4, e1000100.
- Theiler, J., Eubank, S., Longtin, A., Galdrikian, B., & Farmer, J. D. (1992). Testing for nonlinearity in time series: The method of surrogate data. *Physica D: Nonlinear Phenomena*, 58, 77–94.
- Tomasi, D., Wang, G. J., & Volkow, N. D. (2013). Energetic cost of brain functional connectivity. *Proceedings of the National Academy of Sciences of the United States of America*, 110, 13642–13647.

- Tzourio-Mazoyer, N., Landeau, B., Papathanassiou, D., Crivello, F., Etard, O., Delcroix, N., ... Joliot, M. (2002). Automated anatomical labeling of activations in SPM using a macroscopic anatomical parcellation of the MNI MRI single-subject brain. *NeuroImage*, *15*, 273–289.
- van den Heuvel, M. P., de Lange, S. C., Zalesky, A., Seguin, C., Yeo, B. T., & Schmidt, R. (2017). Proportional thresholding in resting-state fMRI functional connectivity networks and consequences for patient-control connectome studies: Issues and recommendations. *NeuroImage*, *152*, 437–449.
- van den Heuvel, M. P., & Sporns, O. (2013). Network hubs in the human brain. *Trends in Cognitive Sciences*, *17*, 683–696.
- Van Dijk, K. R., Sabuncu, M. R., & Buckner, R. L. (2012). The influence of head motion on intrinsic functional connectivity MRI. *NeuroImage*, *59*, 431–438.
- van Wijk, B. C., Stam, C. J., & Daffertshofer, A. (2010). Comparing brain networks of different size and connectivity density using graph theory. *PLoS One*, *5*, e13701.
- Wang, J., Wang, L., Zang, Y., Yang, H., Tang, H., Gong, Q., ... He, Y. (2009). Parcellation-dependent small-world brain functional networks: A resting-state fMRI study. *Human Brain Mapping*, *30*, 1511–1523.
- Wang, J., Wang, X., Xia, M., Liao, X., Evans, A., & He, Y. (2015). GREYNA: A graph theoretical network analysis toolbox for imaging connectomics. *Frontiers in Human Neuroscience*, *9*, 386.
- Wang, Y., Du, H., Xia, M., Ren, L., Xu, M., Xie, T., ... He, Y. (2013). A hybrid CPU-GPU accelerated framework for fast mapping of high-resolution human brain connectome. *PLoS One*, *8*, e62789.
- Wang, Z., Xia, M., Dai, Z., Liang, X., Song, H., He, Y., & Li, K. (2015). Differentially disrupted functional connectivity of the subregions of the inferior parietal lobule in Alzheimer's disease. *Brain Structure & Function*, *220*, 745–762.
- Wang, Z., Yan, C., Zhao, C., Qi, Z., Zhou, W., Lu, J., ... Li, K. (2011). Spatial patterns of intrinsic brain activity in mild cognitive impairment and Alzheimer's disease: A resting-state functional MRI study. *Human Brain Mapping*, *32*, 1720–1740.
- Watts, D. J., & Strogatz, S. H. (1998). Collective dynamics of 'small-world' networks. *Nature*, *393*, 440–442.
- Wig, G. S., Schlaggar, B. L., & Petersen, S. E. (2011). Concepts and principles in the analysis of brain networks. *Annals of the New York Academy of Sciences*, *1224*, 126–146.
- Xia, M., Wang, J., & He, Y. (2013). BrainNet viewer: A network visualization tool for human brain connectomics. *PLoS One*, *8*, e68910.
- Xia, M., Wang, Z., Dai, Z., Liang, X., Song, H., Shu, N., ... He, Y. (2014). Differentially disrupted functional connectivity in posteromedial cortical subregions in Alzheimer's disease. *Journal of Alzheimer's Disease*, *39*, 527–543.
- Yan, C., & Zang, Y. (2010). DPARSF: A MATLAB toolbox for "pipeline" data analysis of resting-state fMRI. *Frontiers in Systems Neuroscience*, *4*, 13.
- Yan, C. G., Cheung, B., Kelly, C., Colcombe, S., Craddock, R. C., Di Martino, A., ... Milham, M. P. (2013). A comprehensive assessment of regional variation in the impact of head micromovements on functional connectomics. *NeuroImage*, *76*, 183–201.
- Yan, C. G., Craddock, R. C., He, Y., & Milham, M. P. (2013). Addressing head motion dependencies for small-world topologies in functional connectomics. *Frontiers in Human Neuroscience*, *7*, 910.
- Yang, G. J., Murray, J. D., Repovs, G., Cole, M. W., Savic, A., Glasser, M. F., ... Anticevic, A. (2014). Altered global brain signal in schizophrenia. *Proceedings of the National Academy of Sciences of the United States of America*, *111*, 7438–7443.
- Zalesky, A., Fornito, A., & Bullmore, E. (2012). On the use of correlation as a measure of network connectivity. *NeuroImage*, *60*, 2096–2106.
- Zalesky, A., Fornito, A., Harding, I. H., Cocchi, L., Yucel, M., Pantelis, C., & Bullmore, E. T. (2010). Whole-brain anatomical networks: Does the choice of nodes matter? *NeuroImage*, *50*, 970–983.
- Zhao, T., Xu, Y., & He, Y. (2018). Graph theoretical modeling of baby brain networks. *NeuroImage*, doi: 10.1016/j.neuroimage.2018.06.038
- Zhao, X., Liu, Y., Wang, X., Liu, B., Xi, Q., Guo, Q., ... Wang, P. (2012). Disrupted small-world brain networks in moderate Alzheimer's disease: A resting-state fMRI study. *PLoS One*, *7*, e33540.
- Zhong, S., He, Y., & Gong, G. (2015). Convergence and divergence across construction methods for human brain white matter networks: An assessment based on individual differences. *Human Brain Mapping*, *36*, 1995–2013.

## SUPPORTING INFORMATION

Additional supporting information may be found online in the Supporting Information section at the end of the article.

**How to cite this article:** Chen X, Liao X, Dai Z, et al. Topological analyses of functional connectomics: A crucial role of global signal removal, brain parcellation, and null models. *Hum Brain Mapp.* 2018;39:4545–4564. <https://doi.org/10.1002/hbm.24305>